

Hydrogen Separation Membranes

Annual Report for FY 2009

Energy Systems Division

About Argonne National Laboratory

Argonne is a U.S. Department of Energy laboratory managed by UChicago Argonne, LLC under contract DE-AC02-06CH11357. The Laboratory's main facility is outside Chicago, at 9700 South Cass Avenue, Argonne, Illinois 60439. For information about Argonne and its pioneering science and technology programs, see www.anl.gov.

Availability of This Report

This report is available, at no cost, at <http://www.osti.gov/bridge>. It is also available on paper to the U.S. Department of Energy and its contractors, for a processing fee, from:

U.S. Department of Energy

Office of Scientific and Technical Information

P.O. Box 62

Oak Ridge, TN 37831-0062

phone (865) 576-8401

fax (865) 576-5728

reports@adonis.osti.gov

Disclaimer

This report was prepared as an account of work sponsored by an agency of the United States Government. Neither the United States Government nor any agency thereof, nor UChicago Argonne, LLC, nor any of their employees or officers, makes any warranty, express or implied, or assumes any legal liability or responsibility for the accuracy, completeness, or usefulness of any information, apparatus, product, or process disclosed, or represents that its use would not infringe privately owned rights. Reference herein to any specific commercial product, process, or service by trade name, trademark, manufacturer, or otherwise, does not necessarily constitute or imply its endorsement, recommendation, or favoring by the United States Government or any agency thereof. The views and opinions of document authors expressed herein do not necessarily state or reflect those of the United States Government or any agency thereof, Argonne National Laboratory, or UChicago Argonne, LLC.

Hydrogen Separation Membranes

Annual Report for FY 2009

prepared by
U. (Balu) Balachandran, S.E. Dorris, Y. Lu, J.E. Emerson,
C.Y. Park, T.H. Lee, and J.J. Picciolo
Energy Systems Division, Argonne National Laboratory

January 30, 2010

Work Supported by
U.S. Department of Energy
Office of Fossil Energy, National Energy Technology Laboratory

Contents

I.	Objective	1
II.	Highlights.....	1
III.	Introduction.....	2
IV.	Results.....	3
	Milestone 1. Test cyclability of membrane vs. temperature and H ₂ concentration in feed gas.	3
	Milestone 2. Measure flux of thin film membrane according to NETL test protocol.....	11
	Additional. Improve density of thin-film membranes....	15
	Additional. Determine the Pd/Pd ₄ S phase boundary at low temperatures (≤600°C) and low H ₂ concentrations (≤10% H ₂).....	20
V.	Future Work.....	27
VI.	Publications and Presentations.....	28
	References.....	34

Figures

1. Scanning electron images of hot-pressed ANL-3e disk after polishing, after annealing for 12 h in flowing He at 500°C, and after annealing for 120 h in flowing He at 850°C.....	6
2. Scanning electron images of hot-pressed ANL-3e disk after twelve and after twenty-four thermal cycles between 300°C and 800°C in flowing He.	7
3. Scanning electron images of hot-pressed ANL-3e disk after five and after fifteen cycles between 4% H ₂ /balance He and 90% H ₂ /balance He at 400°C.	7
4. Scanning electron image of hot-pressed ANL-3e disk after five cycles between 4% H ₂ /balance He and 90% H ₂ /balance He at 500°C.....	7
5. Scanning electron images of thin-film samples after sintering, after twenty cycles between 4% H ₂ /balance He and 90% H ₂ /balance He at 500°C, and after sixteen cycles between 350 and 800 °C in flowing He.	9
6. Scanning electron images of thin-film sample after sixteen cycles between 350 and 800 °C in flowing He.	9
7. Hydrogen flux and purity measured during protocol-test at 400°C.	13
8. Hydrogen flux vs. $\Delta p\text{H}_2^{1/2}$ measured at Argonne according to established protocol and measured previously at Argonne and NETL.....	13
9. Hydrogen flux at 600°C vs. $\Delta p\text{H}_2^{1/2}$ for ANL-3e membranes tested previously at Argonne and measured recently with protocol-test sample.....	14
10. Scanning electron images of ANL-3e thin film made with cobalt nitrate and sintered at 1300°C for 4 h in air on alumina substrate	17
11. Scanning electron images of ANL-3e thin film made with cobalt nitrate and sintered at 1225°C for 4 h in air on TZ-3Y substrate.....	18
12. Cross-sectional view of ANL-3e thin film made with cobalt nitrate and sintered at 1160°C on TZ-3Y substrate with manganese oxide.	20
13. Scanning electron images of Pd ₄ S that formed at 500°C on Pd foil in feed with 20 ppm H ₂ S and on ANL-3e disk in feed with 30 ppm H ₂ S.....	21
14. Scanning electron image of ANL-3e cross-section showing interior zone depleted by Pd that diffused to surface to form Pd ₄ S layer after exposure to feed gas with 10% H ₂ /20 ppm H ₂ S at 500°C.	22
15. Pd/Pd ₄ S phase boundary determined experimentally with curves calculated using thermodynamic parameters derived from the experimental data.	23

16. Plan views of hot-pressed ANL-3e disks after preparation and after 96 h at 500°C in 10 ppm H ₂ S in 10% H ₂ /balance He.	24
17. Secondary electron images comparing Pd ₄ S growth on ANL-3e thin films made with cobalt nitrate on TZ-3Y substrate and made without sintering aid on Al ₂ O ₃ substrate.	25
18. Secondary electron images showing Pd ₄ S growth on hot-pressed ANL-3e disk without sintering aid, ANL-3e thin film with manganese oxide sintering aid, and ANL-3e thin film with cobalt nitrate sintering aid.	26

Tables

1. Effect of initial thermal and hydrogen cycling tests with hot-pressed ANL-3e membranes.	8
2. Hydrogen flux and helium leakage during cycling of ANL-3e thin film membrane between He and “syngas” (50%H ₂ /31%CO ₂ /1%CO/16.25% He)	10
3. Experimental conditions and helium and hydrogen concentrations measured during shake-down experiment of reactor for conducting flux measurements according to established protocol.	12
4. Hydrogen flux and purity measured during shake-down experiment of reactor for conducting permeation measurements according to established protocol.	12
5. Effect of various additives on sintering behavior of ANL-3e thin-film membranes on porous alumina substrates.	16
6. Effect of various sintering aids on densification of porous TZ-3Y substrates.	18
7. Results from fabricating ANL-3e thin films on porous TZ-3Y substrates with sintering aid in both substrate and thin film.	19
8. Summary of Pd/Pd ₄ S phase boundary study with ANL-3e thin films.	25

HYDROGEN SEPARATION MEMBRANES -- ANNUAL REPORT FOR FY 2009

ARGONNE NATIONAL LABORATORY

Project Title: Development of Dense Ceramic Membranes for Hydrogen Separation

NETL Project Manager: Richard Dunst

ANL Project PI: U. (Balu) Balachandran

B&R Code/Contract Number: AA-10-40-00-0/FWP 49601

Report Date: January 30, 2010

I. OBJECTIVE

The objective of this work is to develop dense ceramic membranes for separating hydrogen from other gaseous components in a nongalvanic mode, i.e., without using an external power supply or electrical circuitry.

II. HIGHLIGHTS

1. Our program was reviewed at the 2009 Fuels Peer Review on February 23-27, 2009 in Pittsburgh, PA, and we responded to comments from the reviewers.

2. Milestone 1 was achieved. ANL-3e membranes were found to withstand cycling of temperature and hydrogen concentration in the feed gas without exhibiting significant changes in microstructure or performance.

3. Milestone 2 was achieved. Thin ANL-3e membranes were tested at 400-600°C according to the test protocol established at a contractors' review meeting on April 29, 2008 at Morgantown, WV.

4. Thin ANL-3e membranes are being tested according to the established protocol.

5. With the help of sintering aids, the sintering temperature of ANL-3e thin-film membranes was reduced from $\approx 1400-1450^\circ\text{C}$ to $1160-1210^\circ\text{C}$. Reducing the sintering temperature helps to prevent evaporation of Pd during sintering.

6. The Pd/Pd₄S phase boundary was determined at temperatures of 500-600°C in feed gas with various concentrations of H₂S in 10% H₂/balance He.

7. Various ANL-3e membranes (sintered and hot-pressed disks made without sintering aids and thin films made with and without sintering aids) gave consistent results regarding the Pd/Pd₄S phase boundary but exhibited different kinetics of Pd₄S formation.

III. INTRODUCTION

The goal of this project is to develop dense hydrogen transport membranes (HTMs) that nongalvanically (i.e., without electrodes or external power supply) separate hydrogen from gas mixtures at commercially significant fluxes under industrially relevant operating conditions. HTMs will be used to separate hydrogen from gas mixtures such as the product streams from coal gasification, methane partial oxidation, and water-gas shift reactions. Potential ancillary uses of HTMs include dehydrogenation and olefin production, as well as hydrogen recovery in petroleum refineries and ammonia synthesis plants, the largest current users of deliberately produced hydrogen. This report describes the results from the development and testing of HTM materials during FY 2009.

Materials development for the HTM has followed a three-pronged approach at Argonne. In one approach, we utilized principles of solid-state defect chemistry to properly dope selected monolithic electronic/protonic conductors (perovskites doped on both A- and B-sites) and to obtain materials that are chemically stable and have suitable protonic and electronic conductivities. The second approach used cermet (i.e., ceramic/metal composite) membranes that are prepared by homogeneously mixing electronic/protonic conductors with a metallic component. The metal phase in the cermets enhanced the hydrogen permeability of the ceramic phase by increasing the electronic conductivity and by providing an additional transport path for the hydrogen if the metal has high hydrogen permeability. In our third approach, we dispersed a metal with high hydrogen permeability (called a “hydrogen transport metal”) in a support matrix composed of either a ceramic or a metal. In these composites, hydrogen is transported almost exclusively through the hydrogen transport metal, and the matrix serves primarily as a chemically stable structural support. We focused during FY 2009 on the development of HTMs in which a ceramic phase provided structural support for a hydrogen transport metal. In particular, we focused on “ANL-3e membranes” (composed of Pd mixed with Y₂O₃-stabilized ZrO₂), which have given the highest hydrogen flux to date for membranes made at Argonne (≈ 26 and ≈ 50 cm³/min-cm² at 400 and 900°C, respectively). Various membranes developed at Argonne are summarized elsewhere [1].

In addition to providing high hydrogen flux, HTMs must have sufficient mechanical strength to withstand stresses caused by changes in temperature and feed gas composition. Changes in temperature produce stress in ANL-3e membranes, because they consist of two materials with different coefficients of thermal expansion. Changes in feed gas composition produce stress, because the lattice parameter of Pd depends on the hydrogen concentration in the feed gas. Because HTMs will inevitably encounter changes in temperature and feed gas composition during operation, we have begun evaluating the “cyclability” of ANL-3e membranes, i.e., their ability to withstand the effects of cyclical changes in temperature and feed gas.

Good chemical stability is also a critical requirement for HTMs due to the corrosiveness of product streams from coal gasification and/or methane reforming. Hydrogen sulfide (H₂S) is a particularly corrosive contaminant that HTMs are expected to

encounter. When H₂S reacts with an ANL-3e membrane, palladium sulfide (Pd₄S) forms on the HTM's surface and greatly impedes hydrogen permeation; therefore, the conditions for Pd₄S-formation largely determine a membrane's tolerance for H₂S. We previously used sintered ANL-3e disks to determine the temperatures at which Pd₄S forms in feed gases that contained 10-73% H₂ and ≈8-400 ppm H₂S [2]. We also used Pd foil and hot-pressed ANL-3e disks to locate the Pd/Pd₄S phase boundary at 500-600°C in feed gas with 10% H₂/balance He [2, 3]. To correlate the phase boundary data with the effects of H₂S on the performance of Pd-containing HTMs, we measured the hydrogen flux for commercial Pd foils and ANL-3e membranes during their exposure to feed gas whose H₂S concentration was gradually increased. We report here our study of the Pd/Pd₄S phase boundary at low temperatures (500-550°C) using ANL-3e thin-film membranes made with sintering aids, because preliminary results suggested that such membranes might be more resistant to attack from H₂S.

Hydrogen transport membranes must also have good mechanical integrity at high temperature (≈900°C) and high pressure (≈350 psi). Argonne HTMs have been tested in high-pressure tests at the National Energy Technology Laboratory (NETL) [1] and at Argonne. In tests using Argonne's high-pressure reactor, the hydrogen flux of disk-shaped, self-supported ANL-3e samples was measured in feed gas that contained either 4% H₂ or 90% H₂ at temperatures up to 900°C and pressures up to ≈300 psig [2]. The reactor has since been modified to allow thin-film HTMs (thickness ≈25-50 μm) on porous supports to be tested according to criteria established at NETL. To aid the development of HTMs that satisfy the requirements described above, the following milestones were established in our Field Work Proposal for FY 2009:

1. Test cyclability of membrane vs. temperature and H₂ concentration in feed gas.
2. Measure flux of thin film membrane according to NETL test protocol.

Both milestones for FY 2009 were met in studies using membranes that were developed at Argonne. In addition to meeting these milestones, we identified sintering aids that improve densification of ANL-3e thin-film membranes at lower sintering temperatures, and we continued investigating the Pd/Pd₄S phase boundary at low temperatures (≤600°C) and low H₂ concentrations (≤10% H₂).

IV. RESULTS

Results obtained during FY 2009 are presented below in relation to the pertinent milestone. Work that was done outside the scope of the milestones is also described.

Milestone 1. Test cyclability of membrane vs. temperature and H₂ concentration in feed gas.

The cyclability of ANL-3e membranes was tested with hot-pressed and thin-film samples. To prepare hot-pressed samples, Pd powder (60 vol.%) from Technic, Inc., was mixed with TZ-3Y (ZrO₂ partially stabilized with Y₂O₃) powder from Tosoh Corp. Disks were made by hot-pressing (25 min at 1125-1150°C) the powder mixture under a roughing

pump vacuum. Both sides of the disk were polished with 600-grit SiC polishing paper. After polishing, the disk (thickness of $\approx 150\text{-}175\ \mu\text{m}$) was cleaned with acetone and de-ionized water in an ultrasonic bath.

We prepared ANL-3e thin-films from a powder mixture of Pd (50-60 vol. %) and TZ-3Y (Sigma-Aldrich Co., partially stabilized ZrO_2 , submicron particle size) with either manganese oxide or cobalt nitrate added as a sintering aid. Blending the powder mixture with an organic binder and solvent produced an ink that was used to paint a thin film onto a pre-sintered substrate. After the substrate was painted with the ink, it was dried in air and then sintered for 4-6 h at $1160\text{-}1230^\circ\text{C}$ in air. Substrates were prepared by mixing alumina hydrate powder (Sasol) or TZ-3Y powder (Sigma-Aldrich) with 5-10 mol. % of a sintering aid (relative to alumina or TZ-3Y) and an organic binder. Either carbon black (Fisher Scientific Inc.) or poly(methyl methacrylate-co-ethylene glycol dimethacrylate), PMMA-CE (Sigma-Aldrich, $8\ \mu\text{m}$) were added (20 wt. %) as pore formers, and the powder mixture was uniaxially pressed (5-7 kpsi) into a disk. The pore formers were eliminated by pre-sintering (6-8 h at $900\text{-}950^\circ\text{C}$ in air) the disk.

During cycling tests, samples were held in either an open tray or a spring-loaded test fixture used for measuring hydrogen permeation. During thermal cycling tests, a sample was heated to 300°C at a rate of $3\text{-}4^\circ\text{C}/\text{min}$ and held for 30 min at 300°C , then the temperature was cycled between “end temperatures” of 300°C and 800°C at a ramp rate of $3^\circ\text{C}/\text{min}$ with 30-min dwell periods at each end temperature. After a certain number of cycles, the reactor was cooled to room temperature at a rate of $3\text{-}4^\circ\text{C}/\text{min}$. High purity He flowed through the furnace at a rate of $\approx 120\ \text{ml}/\text{min}$ during the entire test.

In “hydrogen cycling” experiments on a permeation fixture, a sample was slowly heated ($3\text{-}4^\circ\text{C}/\text{min}$) to 400°C or 500°C and held at that temperature for at least 30 min (sometimes overnight). During this period, high purity He flowed ($\approx 150\ \text{ml}/\text{min}$) over one face of the disk while high purity N_2 flowed ($50\ \text{ml}/\text{min}$) over the other side. After the temperature stabilized at 400°C or 500°C , the feed gas composition was cycled between 4% H_2 /balance He and 90% H_2 /balance He. The feed gas flow rate ($\approx 150\text{-}175\ \text{ml}/\text{min}$) was checked during the tests and adjusted, if necessary, with calibrated flow meters (Agilent Optiflow 630 and 570).

The feed gas in hydrogen cycling tests was varied between “end compositions” of 4% H_2 /balance He and 90% H_2 /balance He. A gas flowed for 45-55 min before the feed was switched to the other gas. With a feed gas flow rate of $\approx 150\ \text{ml}/\text{min}$ and furnace volume of $\approx 2600\ \text{ml}$, a feed gas had to flow $\approx 15\text{-}20\ \text{min}$ just to purge the furnace tube. During the transition from one feed gas to the other, we were not certain how much time was required to reach the new composition, but we expected that the new composition would be reached before the end of the dwell. At the end of each day, the feed gas was switched to high purity He overnight as a safety precaution. After a certain number of hydrogen cycles had been completed over several days, the feed gas was switched to high purity He, and the sample was cooled to room temperature.

To determine if cycling caused an increase in leakage, helium leakage through a sample was measured at room temperature before and after cycling tests. The sample was sealed to a permeation fixture with a rubber “O”-ring and placed into a furnace at room temperature. Helium was flowed over the “feed side” of the sample, and N₂ was flowed over the “sweep side,” while a gas chromatograph (GC) measured the He concentration in the sweep gas. The microstructure of samples was studied before and after cycling with scanning electron microscopy (SEM, JEOL 5400) and energy dispersive spectroscopy (EDS) with a Voyager system from Thermo Electron Scientific Instruments Corp.

In some tests with thin-film membranes, the hydrogen flux and helium leakage were measured during hydrogen cycling, in which case the sample was held by a spring-loaded test fixture using a gold ring to form a gas-tight seal between the sample and fixture. The sample was slowly heated (2-3°C/min) to 920°C overnight to improve the seal. High purity helium was flowed on one side of the sample while it was heated, and high purity nitrogen was flowed on the other side.

After a gas seal was made at 920°C, the temperature was reduced to 400°C, and the hydrogen flux and helium leakage were measured while the feed gas was cycled between compositions. Each cycle began in the morning by flowing 4% H₂/balance He at a rate of 150 ml/min for 30-50 min. The feed gas composition was then switched by flowing “coal gas” (50% H₂/31% CO₂/1% CO/16.25% He) at a rate of 160 ml/min. Ultra high purity nitrogen flowing at 150 ml/min was used as the sweep gas. After the sample permeation was measured under these conditions for 5-7 h, the reactor was purged for 25-30 min with 4% H₂/balance He flowing at 150 ml/min. The feed gas was switched overnight to He flowing at 80 ml/min. This cycle was repeated eight times at 400°C, then the temperature was raised to 500°C, and the cycle was repeated five times.

The sweep gas was analyzed two or three times each day with a GC to determine the hydrogen flux and helium leakage. To maintain steady gas flow conditions, gas flow rates were measured with a gas flow rate meter (Agilent 630) and adjusted accordingly after each analysis of the sweep gas. Mass flow controllers (MKS 1179A) were used to blend “coal gas” (61.68% H₂/37.12% CO₂/1.2% CO) and ultra purity helium (99.998%), from Airgas Inc. The reactor had an interior volume of ≈2600 cm³; therefore, ≈15 min was considered sufficient time to switch from one gas composition to another.

Figure 1 shows polished hot-pressed samples before and after annealing at 500°C. These samples did not undergo either thermal or hydrogen cycling and serve as a reference for samples that were cycled. The reference samples shown in Fig. 1 were polished like hot-pressed samples that were either cycled or annealed without cycling. Figure 2 shows a sample after thermal cycling twelve times (Fig. 2a) or twenty-four times (Fig. 2b) between 300°C and 800°C in flowing He. Figure 3 shows samples after cycling at 400°C either five (Fig. 3a) or fifteen (Fig. 3b) times between 4% H₂/balance He and 90% H₂/balance He, while the sample in Fig. 4 underwent five hydrogen cycles between 4% H₂/balance He and 90% H₂/balance He at 500°C. Table 1 summarizes changes in microstructure that were seen after various anneals and cycling tests with hot-pressed samples.

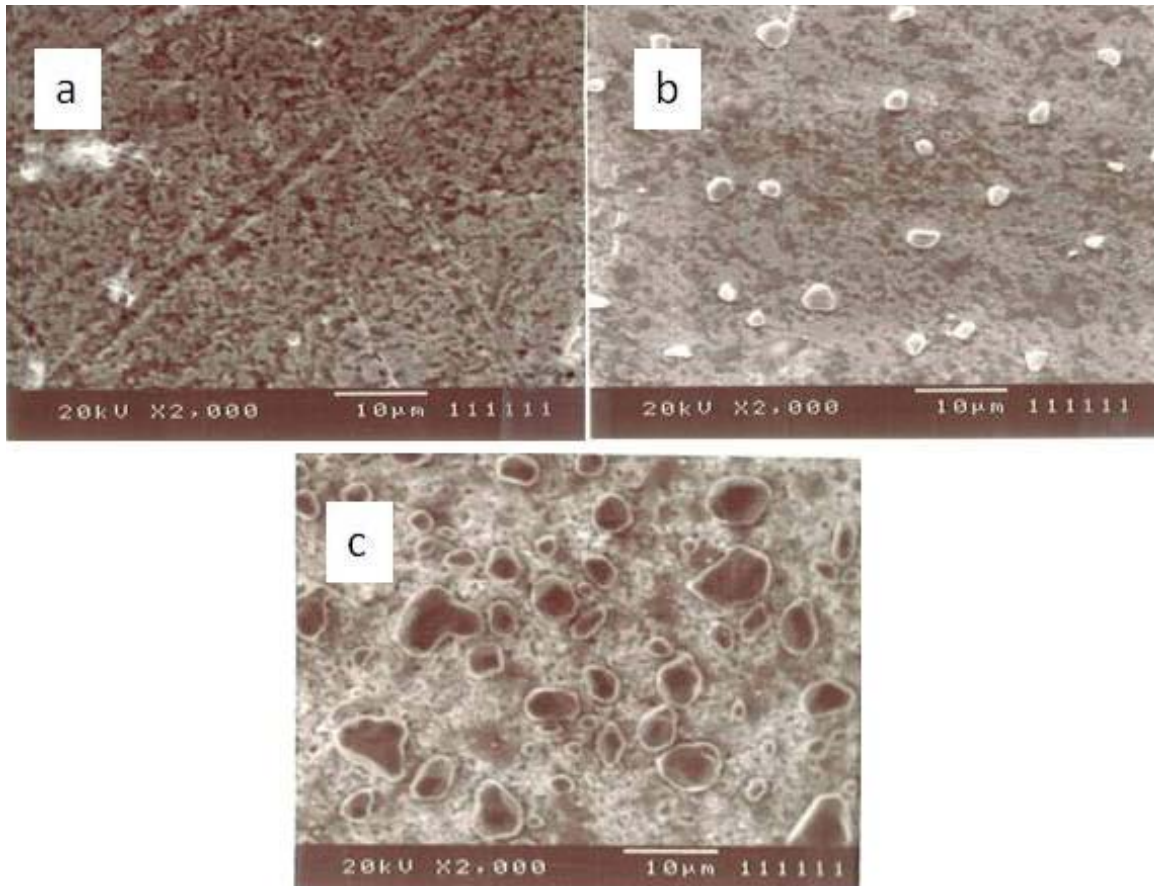


Fig. 1. Scanning electron images of hot-pressed ANL-3e disks a) after polishing and before annealing, b) after annealing for 12 h in flowing He at 500°C, and c) after annealing for 120 h in flowing He at 850°C. Particles on surface are Pd.

A polished, hot-pressed sample exhibited scratches, but particles were not evident (Fig. 1a), whereas particles with diameter of $<2\text{-}3\ \mu\text{m}$ were dispersed over the entire surface of a sample that was annealed for 12 h at 500°C (Fig. 1b). Particles were also seen on a sample that was annealed for a longer period (120 h) at higher temperature (850°C), but the particles were larger and more numerous (Fig. 1c). Similar-looking particles were also dispersed over the entire surface of samples that underwent thermal cycling (Fig. 2) or hydrogen cycling (Fig. 3), but the size and abundance of the particles varied with details of the cycling tests. When the number of thermal cycles was doubled, the size and concentration of particles increased (Fig. 2). Likewise, the particles grew in size and number when the number of hydrogen cycles at 400°C was tripled (Fig. 3) and when the same number of hydrogen cycles was done at 500°C (Fig. 4) rather than 400°C (Fig. 3a). The EDS results showed that the particles on these various samples contained essentially pure Pd. The growth of such particles was the only discernible change in microstructure after a hot-pressed sample underwent thermal or hydrogen cycling, or it was annealed without cycling.

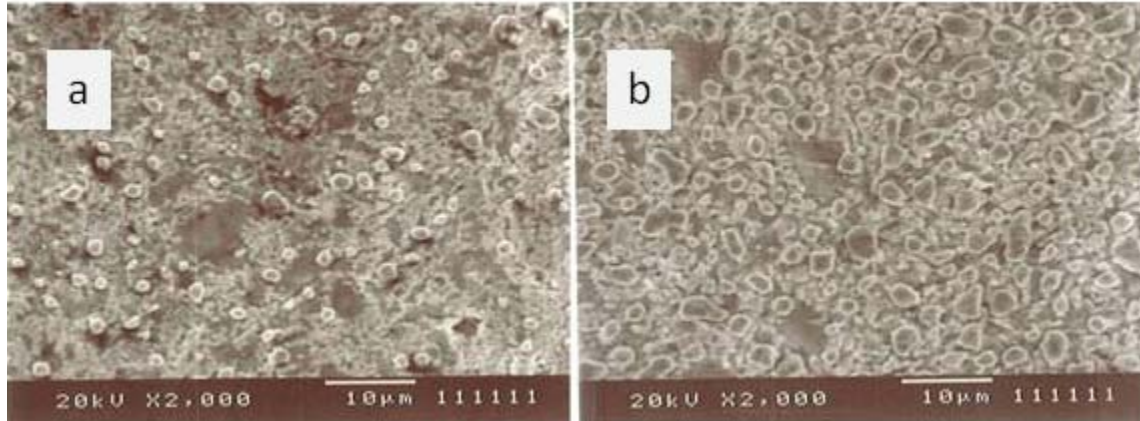


Fig. 2. Scanning electron images of hot-pressed ANL-3e disk after a) twelve and b) twenty-four thermal cycles between 300°C and 800°C in flowing He. Particles on surface are Pd.

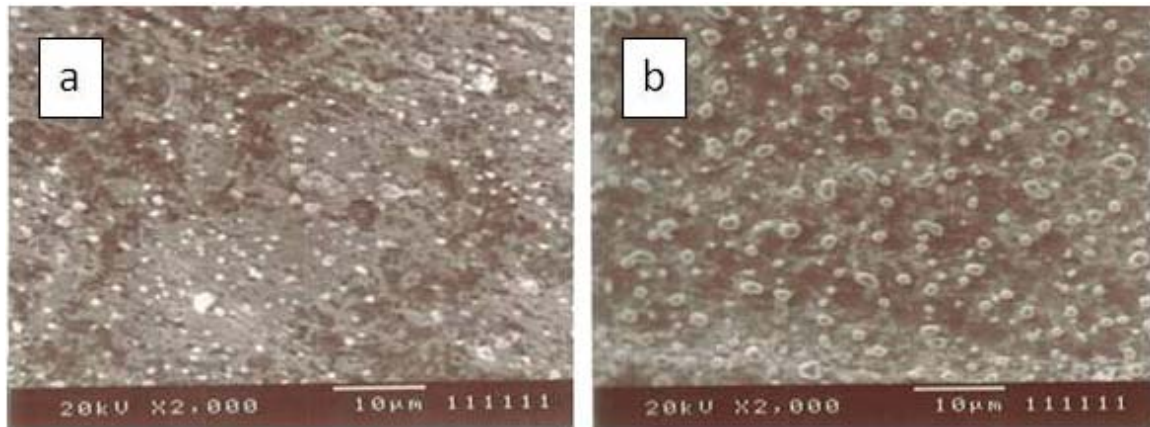


Fig. 3. Scanning electron images of hot-pressed ANL-3e disk after a) five and b) fifteen cycles between 4% H₂/balance He and 90% H₂/balance He at 400°C. Particles on surface are Pd.

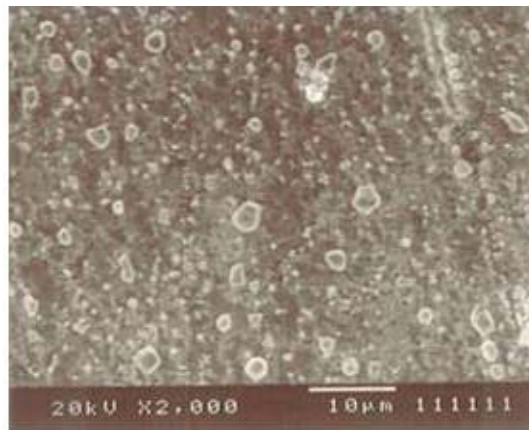


Fig. 4. Scanning electron image of hot-pressed ANL-3e disk after five cycles between 4% H₂/balance He and 90% H₂/balance He at 500°C. Particles on surface are Pd.

Table 1. Effect of initial thermal and hydrogen cycling tests with hot-pressed ANL-3e membranes [4].

Type of Cycling	Conditions	Results	Microstructure
Anneal No cycling	12 h @ 500°C He	Pd particles on surface	Fig. 1b
Anneal No cycling	120 h @ 850°C He	Pd particles larger, more abundant	Fig. 1c
Thermal	12 cycles 300 - 800°C He	Pd particles on surface	Fig. 2a
Thermal	24 cycles 300 - 800°C He	Pd particles larger, more abundant than after 12 cycles	Fig. 2b
Hydrogen	5 cycles 4% H ₂ - 90% He 400°C	Small Pd particles on surface	Fig. 3a
Hydrogen	15 cycles 4% H ₂ - 90% He 400°C	Pd particles larger than after 5 cycles	Fig. 3b
Hydrogen	5 cycles 4% H ₂ - 90% He 500°C	Pd particles larger than after 5 cycles at 400°C	Fig. 4

Figure 5 shows secondary electron images of as-sintered thin films, i.e., without any type of cycling or anneal (Fig. 5a), after twenty cycles between 4% H₂/balance He and 90% H₂/balance He (Fig. 5b) at 500°C, and after sixteen cycles between 350°C and 800°C in flowing He (Fig. 5c). Although Fig. 5 shows features with size of ≈2-10 μm that might look like the particles on hot-pressed samples (Figs. 1-4), the particle-like features on thin-film samples are fundamentally different from those on hot-pressed samples. The features in Fig. 5 appear less rounded, and smaller features are evident on the particles. A backscattered electron image from a thermally cycled thin film (Fig. 6) revealed both light and dark areas in the apparent particles, indicating a variation in chemical composition. Unlike the nearly pure Pd particles on hot-pressed samples, these features contain a mixture of Pd and TZ-3Y. Most important, the particle-like features on thin-film samples do not change their appearance during cycling tests, looking nearly identical to the features on the as-sintered film.

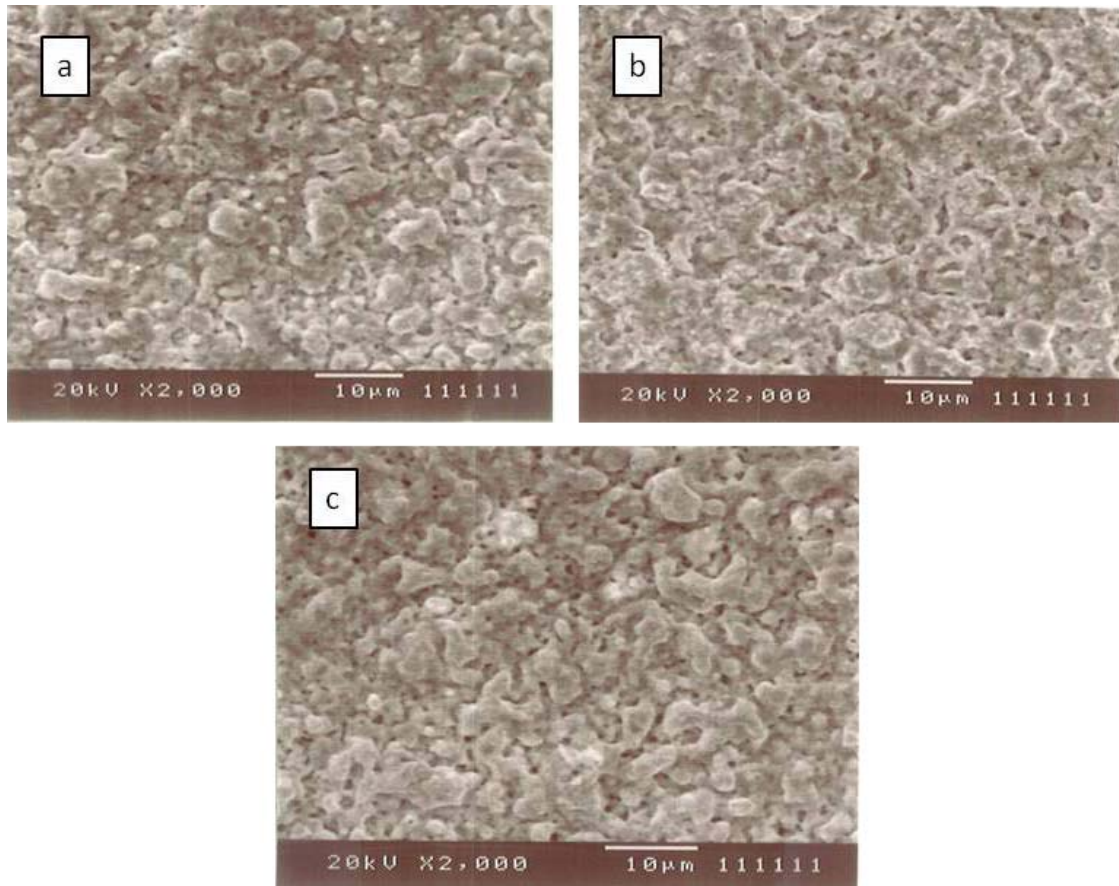


Fig. 5. Secondary electron images of thin-film samples after a) sintering 4-6 h at 1160-1230°C in air, b) twenty cycles at 500°C between 4% H₂/balance He and 90% H₂/balance He, and c) sixteen cycles between 350 and 800 °C in flowing He.

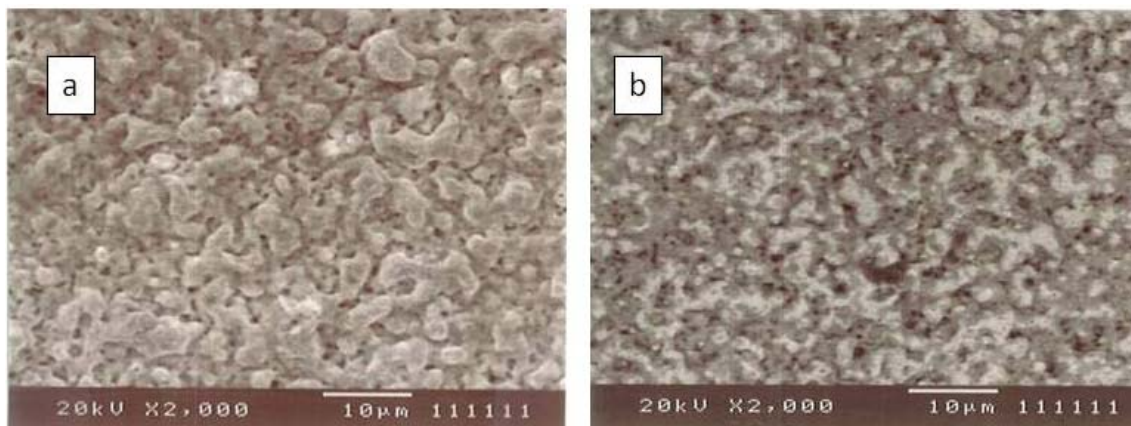


Fig. 6. a) Secondary electron and b) backscattered electron image of thin-film sample after sixteen cycles between 350 and 800 °C in flowing He.

The fact that the size and abundance of Pd particles on hot-pressed samples increased with the number of thermal and hydrogen cycles suggests that cycling contributed to growth of the particles, but Pd particles also appeared on samples that were not cycled (Figs. 1b and 1c). Considering that the particles were comparable in size and abundance whether a sample was cycled or annealed without cycling, it seems unreasonable to attribute the growth of Pd particles to effects from cycling. The fact that all samples had been polished before the particles grew suggests that the particles are an artifact from polishing, and the absence of pure Pd particles on thin-film samples, which were not polished, supports this idea. During polishing, TZ-3Y is removed from the surface due to its brittleness (relative to Pd), but Pd tends to smear across the sample's surface. When a polished sample is subsequently heated during annealing or cycling tests, the Pd left on the surface can reduce its surface energy by coalescing into particles. Coalescence of the Pd was evidently incomplete after briefer tests at lower temperature, because the size and number of particles increased with the number of cycles (Fig. 2a vs. Fig. 2b), the cycling temperature (Fig. 3a vs. Fig. 4), and the duration and temperature of annealing without cycling (Fig. 1b vs. Fig. 1c).

Helium leakage measurements support the idea that polishing, and not cycling, led to the formation of Pd particles on the surface of hot-pressed samples. Helium leakage at room temperature was not detectible before or after the tests. The fact that the helium leakage did not increase during the tests indicates that the amount of interconnected porosity did not increase, because interconnected porosity is necessary for helium leakage, and helium leakage increases with interconnected porosity. If the interconnected porosity did not increase, the particles probably grew from Pd left on the surface after polishing, because Pd transport from the interior would have increased the interconnected porosity.

In summary, neither thermal nor hydrogen cycling caused significant changes in hot-pressed or thin-film ANL-3e samples. The presence of Pd particles on the surface of polished hot-pressed samples was attributed to coalescence of Pd left behind by polishing. Growth of the particles did not noticeably affect helium leakage through the samples. Likewise, *in situ* measurements made during hydrogen cycling (Table 2) of a thin-film sample showed that its hydrogen flux did not change during cycling at 400°C and 500°C. Helium leakage through the sample did not change during cycling at 500°C, and the slight change during cycling at 400°C is within the range of experimental uncertainty.

Table 2 Hydrogen flux (ml/min) and He leakage (ml/min) during cycling of ANL-3e thin-films between “syngas” (50% H₂/31% CO₂/1% CO/16.25% He) and He.

Test	1 st cycle	Last cycle
400 °C, eight cycles between He and “syngas”	Flux: 9.76-10.15 Leakage: 0.034-0.047	Flux: 9.60-10.43 Leakage: 0.054-0.056
500 °C,* five cycles between He and “syngas”	Flux: 11.89-12.15 Leakage: 0.065-0.070	Flux: 11.67-12.02 Leakage: 0.065-0.070

*The 500°C test was carried out right after 400°C test.

Milestone 2. Measure flux of thin film membrane according to NETL test protocol.

A protocol for testing hydrogen separation membranes was developed at a contractors' review meeting on April 29, 2008, at Morgantown, WV. A high-pressure permeation reactor at Argonne was modified for the purpose of testing hydrogen separation membranes according to the established protocol. Results are presented here from a "shake-down" experiment of Argonne's reactor that lasted ≈ 5 h, and a second experiment that lasted ≈ 600 h. Although the second test lasted ≈ 600 h, the sample was exposed to the protocol test conditions for only ≈ 120 h, because the reactor was not approved for unattended operation, and the feed gas had to be switched to helium at the end of each day. After the second test was completed, the reactor was approved for unattended operation. Further tests according to the protocol are underway.

A thin ANL-3e cermet membrane was prepared by hot-pressing a powder mixture of 60 vol.% Pd/40 vol.% TZ-3Y for 25 min at 1125°C . After hot-pressing, the disk was polished to a thickness of 125-150 μm . It was sealed for testing by squeezing it between two Haynes HR-160 alloy tubes using graphite washers to obtain gas-tight seals between the membrane and the HR-160 tubes. The sample was heated to 400°C at a rate of $50^{\circ}\text{C}/\text{h}$ while Ar was flowed on the sweep side of the sample and He on the feed side.

After the temperature reached 400°C , the feed gas composition was switched to 50.3% H_2 , 1.0% CO , 30.2% CO_2 , and 18.5% H_2O . The feed gas composition changed to 47.4% H_2 , 0.9% CO , 28.4% CO_2 , 17.4% H_2O , and 5.9% He when He was added for measuring leakage. To compare the performance of samples tested according to the protocol to that of samples tested previously, the flux was measured over the temperature range $400\text{-}600^{\circ}\text{C}$ with feed gas of $\approx 90\%$ H_2 /balance He (feed pressure $\approx 3\text{-}7$ psig) at the end of the second test. The hydrogen and helium concentrations in the sweep gas were measured with a GC four times every hour to calculate the hydrogen flux. According to the test protocol, the feed gas should be fully analyzed as it exits the reactor, which is possible in principle but requires the GC and the GC operator to be dedicated solely to this experiment. Under the present circumstances, this arrangement is not possible; therefore, the H_2 , He, CO , and CO_2 concentrations were measured only at the beginning of the day and at the end of the day. During the day, only the H_2 and He concentrations were measured. Unless personnel and a new GC can be added, a similar procedure will be followed during typical future runs.

Table 3 shows the hydrogen and helium concentrations that were measured in the sweep stream during the shake-down experiment that lasted five hours, and Table 4 shows the hydrogen flux and purity that were calculated from the measured hydrogen and helium concentrations. Figure 7 plots the values of hydrogen flux and purity that were measured in the second experiment. The Excel spreadsheet that was used to calculate the hydrogen flux and purity is available upon request. Figures 8 and 9 compare the hydrogen flux values measured in the second experiment to values that were measured previously with other samples. To compare values from samples with various thicknesses, we normalized all values in Figs. 8 and 9 to a thickness of 20 μm .

Table 3. Experimental conditions and helium and hydrogen concentrations measured at 400°C during shake-down experiment of reactor for conducting permeation measurements according to established protocol.

Time (h)	Sweep Flowrate (ml/min)	P _{Feed} (psig)	P _{Sweep} (psig)	He Leakage (%)	H ₂ Conc. (%)
40.988	216.50	206.41	22.76	0.0052	1.7880
41.050	216.50	206.41	22.76	0.0042	1.7855
41.140	216.50	206.41	22.76	0.0069	1.7935
41.281	216.50	206.41	22.76	0.0055	1.8029
41.941	217.00	206.10	23.10	0.0042	1.7888
42.049	217.00	206.10	23.10	0.0039	1.8049
42.126	217.00	206.10	23.10	0.0000	1.8373
42.215	217.00	206.10	23.10	0.0042	1.7988
42.868	216.25	202.89	23.09	0.0034	1.8144
42.950	216.25	202.89	23.09	0.0040	1.8052
43.027	216.25	202.89	23.09	0.0042	1.8159
43.096	216.25	202.89	23.09	0.0040	1.7684
43.782	215.75	202.94	22.89	0.0029	1.6544
43.852	215.75	202.94	22.89	0.0029	1.6525
43.936	215.75	202.94	22.89	0.0031	1.6764
44.007	215.75	202.94	22.89	0.0033	1.6473
44.859	214.25	205.44	22.82	0.0046	1.7907
44.931	214.25	205.44	22.82	0.0043	1.7062
45.005	214.25	205.44	22.82	0.0031	1.7109
45.074	214.25	205.44	22.82	0.0037	1.7055

Table 4. Hydrogen flux and purity measured at 400°C during shake-down experiment of reactor for conducting permeation measurements by established protocol.

Time (h)	He Leakage (%)	H ₂ Conc. (%)	H ₂ Flux (cm ³ /min-cm ²)	"Purity"
40.988	0.0052	1.7880	4.467	99.709
41.050	0.0042	1.7855	4.492	99.765
41.140	0.0069	1.7935	4.428	99.615
41.281	0.0055	1.8029	4.496	99.695
41.941	0.0042	1.7888	4.511	99.765
42.049	0.0039	1.8049	4.562	99.784
42.126	0.0000	1.8373	4.768	100.000
42.215	0.0042	1.7988	4.537	99.767
42.868	0.0034	1.8144	4.586	99.813
42.950	0.0040	1.8052	4.544	99.778
43.027	0.0042	1.8159	4.565	99.769
43.096	0.0040	1.7684	4.449	99.774
43.782	0.0029	1.6544	4.178	99.825
43.852	0.0029	1.6525	4.173	99.825
43.936	0.0031	1.6764	4.229	99.815
44.007	0.0033	1.6473	4.148	99.800
44.859	0.0046	1.7907	4.446	99.743
44.931	0.0043	1.7062	4.239	99.748
45.005	0.0031	1.7109	4.288	99.819
45.074	0.0037	1.7055	4.256	99.783

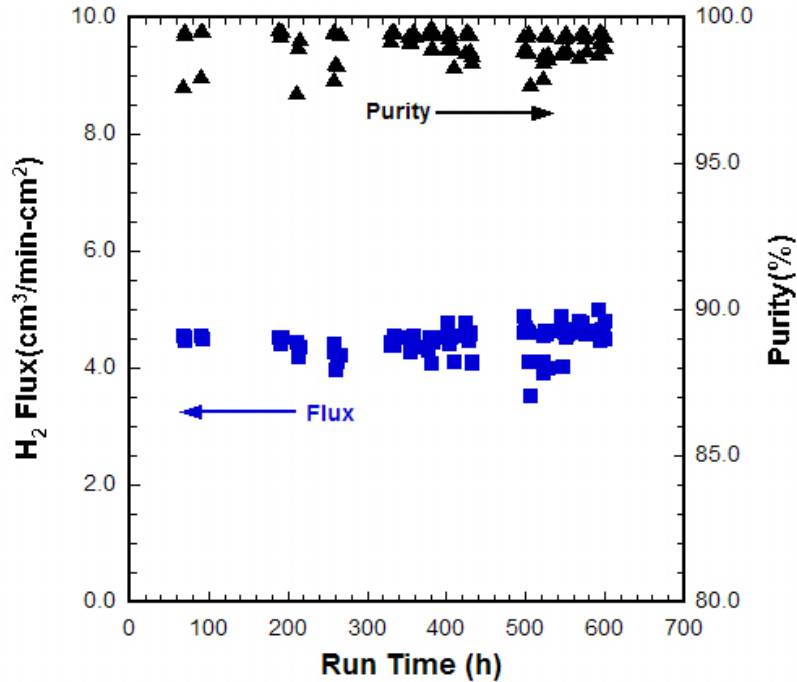


Fig. 7. Hydrogen flux and purity measured during protocol test at 400°C with ANL-3e membrane (thickness $\approx 125\text{-}150\ \mu\text{m}$).

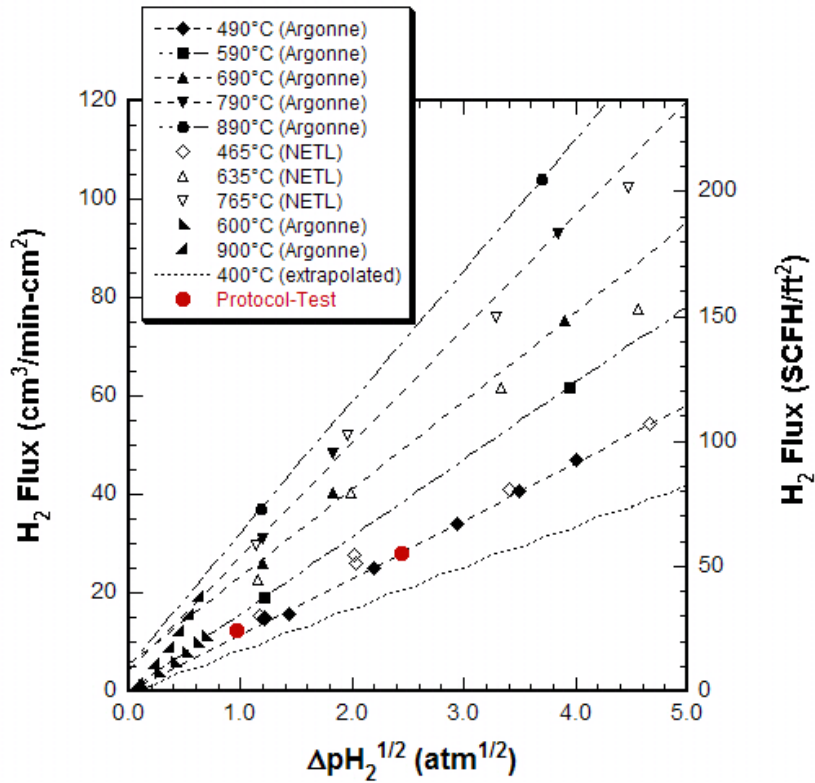


Fig. 8. Hydrogen flux at various temperatures vs. $\Delta p H_2^{1/2}$ (defined in text) for ANL-3e membranes tested at Argonne and NETL [2]. Red symbols give values at 400°C measured at Argonne with protocol-test sample. All values are normalized to a membrane thickness of 20 μm .

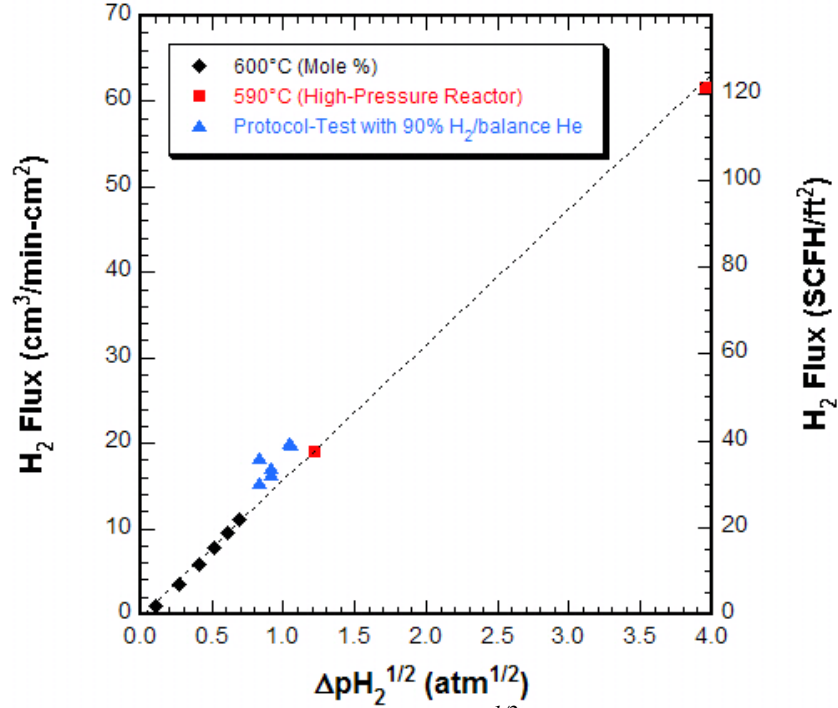


Fig. 9. Hydrogen flux at 600°C vs. $\Delta p\text{H}_2^{1/2}$ (defined in text) for ANL-3e membranes tested previously at Argonne and measured with protocol-test sample. All values normalized to thickness of 20 μm .

Figures 8 and 9 plot the hydrogen flux over a range in temperatures versus $\Delta p\text{H}_2^{1/2}$, which is defined in terms of the partial pressures of hydrogen on the feed and sweep sides of the membrane:

$$\Delta p\text{H}_2^{1/2} \equiv \sqrt{p\text{H}_2(\text{feed})} - \sqrt{p\text{H}_2(\text{sweep})} \quad (6)$$

Figure 8 shows data collected previously [2] at NETL and Argonne and values that were measured in the protocol tests. Flux was measured at $\Delta p\text{H}_2^{1/2} < 1 \text{ atm}^{1/2}$ by varying the feed composition while maintaining a total pressure of 1 atm. Values were measured at $\Delta p\text{H}_2^{1/2} > 1 \text{ atm}^{1/2}$ by varying total pressure with the feed composition fixed at 90% H_2 /balance He. Values measured previously at Argonne were extrapolated to 400°C, the temperature of the protocol tests assuming thermally activated permeation through palladium. The two points in red (Fig. 8) were measured with the protocol-test sample. The value at $p\text{H}_2^{1/2} \approx 2.4 \text{ atm}^{1/2}$ was measured under the protocol conditions, and the value at $\Delta p\text{H}_2^{1/2} \approx 1 \text{ atm}^{1/2}$ was measured using a feed gas of $\approx 90\%$ H_2 /balance He (pressure $\approx 3\text{-}7$ psig) after completion of the protocol test.

Figure 9 plots hydrogen flux values measured previously at Argonne at 590°C by varying the total pressure while fixing the feed composition at 90% H_2 /balance He, and at 600°C by varying the feed composition while maintaining a total pressure of 1 atm. Also shown are values measured with the protocol-test sample using 90% H_2 /balance He (pressure $\approx 3\text{-}7$ psig) as the feed gas. Six values are reported for the protocol-test sample, for which the flux was measured at sweep gas flow rates from ≈ 200 to ≈ 1000 ml/min. As the sweep flow rate increased, $p\text{H}_2(\text{sweep})$ decreased and $p\text{H}_2^{1/2}$ increased.

Hydrogen flux values measured with the protocol-test sample were slightly higher than values that were measured previously with similar samples, as seen by comparing the protocol-test values to the extrapolated values at 400°C (Fig. 8) and by comparing values measured at 600°C (Fig. 9). The difference is not significant and is attributed to experimental uncertainties in the measurement of flux and sample thickness. Thickness measurements are a factor because they were used to normalize flux measurements to the same thickness in order to compare flux values for the different samples.

The membranes were examined by SEM after the protocol tests at 400°C. The thickness of the samples was measured to be 125-150 μm . After the shake-down experiment, the sweep side of the sample appeared similar to the as-polished surface, with Pd somewhat smeared across the surface from the polishing process, whereas Pd appeared more like discrete particles on the feed surface. After the longer (≈ 120 h) experiment at 400°C, Pd particles were found on both feed and sweep surfaces. The particles appear to be similar to those found after the cycling and annealing experiments and are likely an artifact from polishing.

The results from the first two “protocol tests” show that Argonne’s reactor is suitable for making measurements according to the established protocol. The method for obtaining gas-tight seals (mechanically loading graphite gaskets between the membrane sample and the tubes that carry the feed and sweep gases) appears satisfactory, as seen by the low He leakage values (Table 3) and high purities (Fig. 7). The quality of the gas seal depends critically on proper positioning of the sample and good alignment between its sealing surface and that of the gas-bearing tubes. As more experience is gained with this sealing method, the quality of the seal seems to be improving; therefore, we believe that lower leakage and higher purity can be achieved in future runs.

Additional Effort: Improve density of thin-film membranes.

Reducing a membrane’s thickness is expected to increase its hydrogen flux; however, reducing its thickness also increases the possibility that it contains pinholes that degrade its selectivity. To avoid formation of pinholes, membranes must have high density. High-density ANL-3e membranes can be made by sintering them at high temperatures ($\geq 1400^\circ\text{C}$), but evaporation of Pd can reduce the Pd content on their surface if the sintering temperature is too high. A Pd-deficient layer can be removed simply by polishing the membrane if it is a self-supporting disk, but polishing can easily damage a thin-film membrane, especially if the film is not flat. To produce high density thin-film membranes while reducing their loss of Pd during sintering, we tested several sintering aids during FY 2009 that allow densification at sintering temperatures $< 1300^\circ\text{C}$. ANL-3e thin films made with nitrates of cobalt, copper, and bismuth were found to densify in the temperature range 1180-1225°C, but they tended to crack or delaminate from Al_2O_3 substrates due to their higher sintering temperature [5]. Thin films made with sintering aids did not delaminate from TZ-3Y substrates, however, due to the lower sintering temperature of TZ-3Y [5].

Nitrates of cobalt, copper, and bismuth have been reported to be effective sintering aids for ZrO₂ [6-8]; therefore, we tested them as sintering aids for ANL-3e thin films on porous substrates made from Al₂O₃ or TZ-3Y. Substrates were prepared by mixing either alumina hydrate powder (Sasol) or TZ-3Y powder (Tosoh) with carbon black powder (Fisher Scientific, 20 wt. %), uniaxially pressing the powder mixture (5-7 kpsi) into a disk, and pre-sintering the disk for 6-8 h at 900-950°C in air. Pre-sintering eliminated the carbon pore former and gave the substrate mechanical integrity for subsequent handling.

A powder mixture for making ANL-3e thin-film membranes was prepared by mixing 50-60 vol. % Pd powder (Technic) with TZ-3Y powder (Tosoh) and one of the additives being tested as a sintering aid (1.3-4.4 mol. %, relative to TZ-3Y). The amount of additive in the mixture was chosen based on the literature [6-8]. Blending the mixture with an organic binder and solvent gave an ink that was used to paint a thin film onto a pre-sintered substrate. Additives were incorporated in the form of nitrates, rather than oxides, because nitrates readily disperse in the ink and form finely divided oxides when they decompose during sintering of the film. After the substrate was painted with a film, it was dried in air and sintered for 4-6 h at 1225-1380°C in air. Sintered films were tested for pinholes and/or microcracks by checking for penetration of the film by isopropyl alcohol (IPA). Penetration of the film by IPA was visible as darkening of the film and indicated cracks or interconnected porosity in film. Microstructures of the films were examined by SEM, and EDS was used to estimate the Pd content on the surface of sintered films.

Table 5 summarizes the findings from tests of ANL-3e films made with sintering aids on alumina substrates. Microstructure examinations and IPA-penetration tests showed that dense films were made at sintering temperatures of 1280-1300°C by using cobalt nitrate, bismuth nitrate, or copper nitrate as a sintering aid. In contrast, samples sintered at 1225-1250°C remained porous. Figure 10 shows micrographs taken from an ANL-3e thin film made with 4.4 mol. % cobalt nitrate and sintered for 4 h at 1300°C in air. The film appeared dense, and EDS showed no noticeable loss of Pd from its surface. In fact, EDS showed no appreciable loss of Pd from samples sintered at temperatures below 1350°C. Films that contained bismuth nitrate or copper nitrate, however, tended to crack or delaminate from the substrate, probably due to a mismatch in shrinkage during sintering.

Table 5. Effect of various additives on sintering behavior of ANL-3e thin-film membranes on porous alumina substrate sintered in air.

Sintering Aid	1225-1250°C	1280-1300°C	1335-1350°C
Cobalt Nitrate (4.4 mol. %)	Porous	Dense Crack free	Dense Crack free
Bismuth Nitrate (2 mol. %)	Porous	Dense Cracks	Not tested
Copper Nitrate (1.3 mol. %)	Porous	Dense Cracks	Not tested

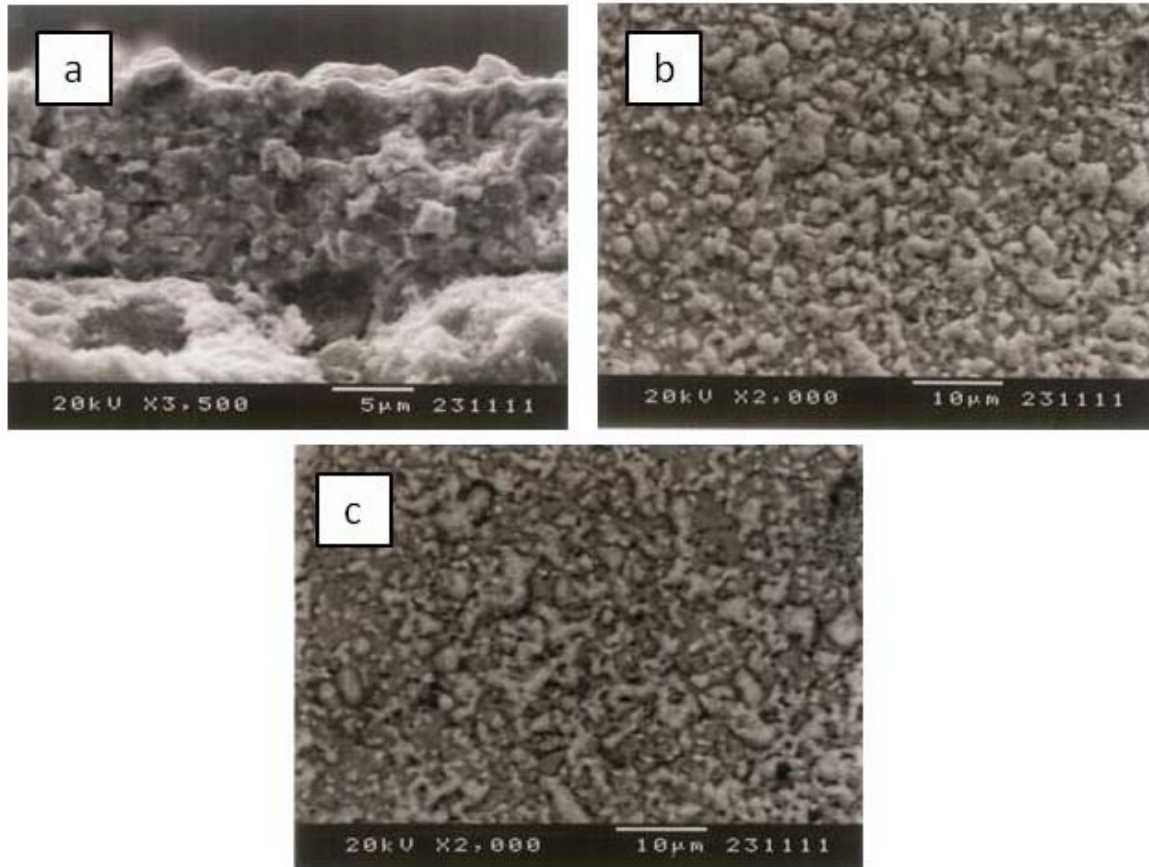


Fig. 10. ANL-3e thin-film membrane made with cobalt nitrate on alumina substrate and sintered in air for 4 h at 1300°C: (a) cross-section, secondary electron image; (b) top view, secondary electron image; (c) same view as (b) but backscattered electron image. Bright area is Pd, and grey area is TZ-3Y phase.

The densification of ANL-3e thin films is strongly affected by the densification of its substrate. When a thin film and its substrate are heated to the sintering temperature, tensile stresses develop in the thin film if it densifies at a lower temperature than does the substrate. If the onset of densification for the substrate differs too greatly from that of the thin film, the tensile stresses can retard densification of the film or cause it to crack or delaminate from the substrate. For these reasons, the sintering behavior of a thin film and its substrate must be compatible. The fact that films made with bismuth nitrate or copper nitrate crack during sintering suggests that these films densify at a lower temperature than does the alumina substrate, and that the sintering temperature of ANL-3e thin films might be reduced below 1280°C by using a substrate that densifies at a lower temperature. Tests indicate that dense ANL-3e thin films can be made at sintering temperatures of 1180-1225°C by using porous TZ-3Y as the substrate and cobalt nitrate as the sintering aid. Figure 11 shows micrographs from an ANL-3e film made with cobalt nitrate on a TZ-3Y substrate and sintered for 4 h at 1225°C in air.

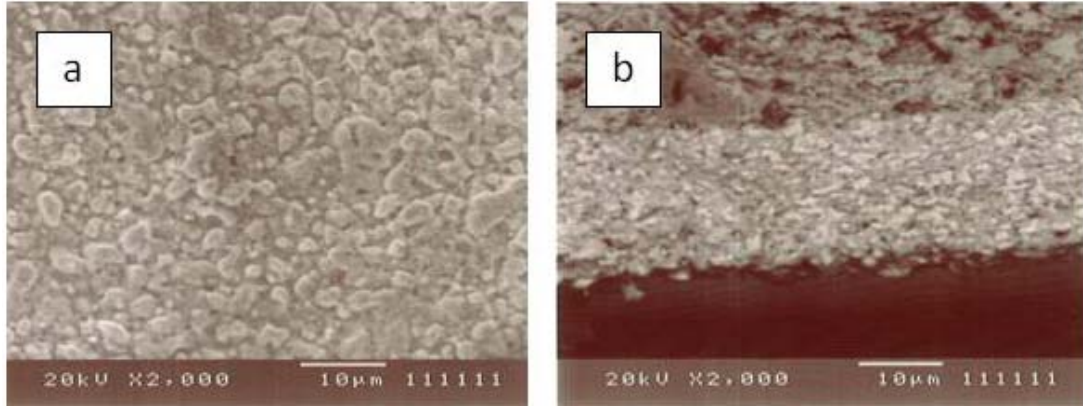


Fig. 11. ANL-3e thin film made with cobalt nitrate on porous TZ-3Y substrate and sintered in air for 4 h at 1225°C: (a) top view, secondary electron image and (b) cross section, backscattered electron image.

To develop a thin film and substrate combination with compatible sintering behavior, we investigated the effect of sintering aids on densification of TZ-3Y substrates. Our experience with ANL-3e thin films showed that the substrates undergo $\approx 25\%$ lateral shrinkage in samples that achieve full densification; therefore, we tested various potential sintering aids to determine materials and sintering conditions that would yield this level of shrinkage in TZ-3Y substrates. Table 6 shows the materials we tested and the results from the tests.

Table 6. Effect of various sintering aids on densification behavior of porous TZ-3Y substrate during sintering in air.

Sintering Aid	Amount (Mol. %)	Results
Cobalt Nitrate	5-6	Sufficient shrinkage above 1210 °C.
Bismuth Nitrate	8	Sufficient shrinkage above 1050°C. Bismuth oxide is volatile and reacts with materials in thin film membrane.
Bismuth Nitrate	4-5	Insufficient substrate shrinkage at $\leq 1180^\circ\text{C}$. Bismuth oxide is volatile and reacts with materials in thin film membrane.
Manganese Oxide	6	Sufficient shrinkage above 1150 °C.
Copper Nitrate	8-10	Sufficient shrinkage above 1210°C. Substrate tends to crack during pre-sintering.

All the materials tested produced sufficient (i.e., $\geq 25\%$) lateral shrinkage in TZ-3Y substrates sintered at temperatures $\geq 1210^\circ\text{C}$, but other problems made some materials unsatisfactory. Bismuth nitrate was volatile and reacted with palladium in the ANL-3e thin film, whereas substrates tended to crack during pre-sintering when copper nitrate was used as a sintering aid. In substrates sintered at 1210°C , cobalt nitrate and manganese oxide both yielded shrinkage that is adequate to densify ANL-3e thin films, but the substrates made with manganese oxide densified at a slightly lower temperature (1150 vs. 1210°C). With a lower sintering temperature, the substrate is less likely to exert tensile forces on the thin film during sintering, and might even assist densification of the thin film by placing it under compression. To further compare cobalt nitrate and manganese oxide as sintering aids, they were used to fabricate thin-film samples in which sintering aids were tested in both the thin film and the substrate.

Table 7 summarizes the results from IPA-penetration tests and SEM examination of samples that were made with cobalt nitrate or manganese oxide as a sintering aid in both the TZ-3Y substrate and the ANL-3e thin film. The results show that ANL-3e thin films with cobalt nitrate on TZ-3Y substrates with manganese oxide were dense when sintered at temperatures $\geq 1160^\circ\text{C}$. Figure 12 shows an example of such a thin film. Slightly higher sintering temperatures ($\geq 1210^\circ\text{C}$) were required to produce dense thin films when cobalt nitrate was used as a sintering aid for both the substrate and thin film. Likewise, a slightly higher sintering temperature ($\geq 1180^\circ\text{C}$) was needed to achieve dense thin films when manganese oxide was used as a sintering aid for both the substrate and thin film. Although a lower sintering temperature should reduce evaporation of Pd from the thin film, the difference in sintering temperatures is probably insignificant. Future tests will compare the hydrogen flux and helium leakage through thin-film membranes made with cobalt nitrate and manganese oxide as the sintering aid.

Table 7. Results from fabricating ANL-3e thin films on porous TZ-3Y substrates with sintering aid (≈ 6 mol.%) added to both substrate and thin film.

Thin-Film Additive	Substrate Additive	Results
Cobalt Nitrate	Manganese Oxide	Porous membrane below 1150°C Dense membrane above 1160°C
Cobalt Nitrate	Cobalt Nitrate	Porous membrane below 1190°C Dense membrane above 1210°C
Manganese Oxide	Manganese Oxide	Porous membrane below 1160°C Dense membrane above 1180°C

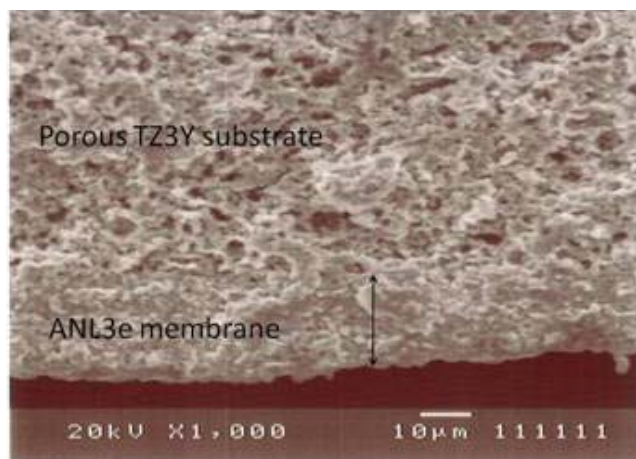


Fig. 12. Cross-sectional view of ANL-3e thin film with cobalt nitrate sintered at 1160°C on porous TZ-3Y substrate with manganese oxide.

Additional Effort: Determine the Pd/Pd₄S phase boundary at low temperatures (≤600°C) and low H₂ concentrations (≤10% H₂).

Due to the corrosive nature of gases that HTMs will contact (e.g., product streams from coal gasification and/or methane reforming), good chemical stability is a critical requirement for HTMs. Hydrogen sulfide (H₂S) is a particularly corrosive contaminant that HTMs are expected to encounter. When H₂S reacts with an ANL-3e membrane, palladium sulfide (Pd₄S) forms on the membrane's surface and greatly impedes hydrogen permeation through the membrane; therefore, a membrane's tolerance for H₂S can be judged by the conditions under which Pd₄S forms. An earlier study [2] determined temperatures at which Pd₄S forms in feed gases with 10-73% H₂ and ≈8-400 ppm H₂S. Other studies [5, 9] determined H₂S concentrations at which Pd₄S forms on Pd foil and hot-pressed ANL-3e disks in feed gas with 10% H₂/balance He at temperatures in the range 500-600°C. Later tests were done with ANL-3e thin-film membranes made with sintering aids, because preliminary results suggested that such membranes might be more resistant to attack from H₂S. This report summarizes our investigation during FY 2009 of the Pd/Pd₄S phase boundary at temperatures in the range 400-600°C.

Samples of Pd foil (Alfa Aesar, thickness = 100 µm) and hot-pressed ANL-3e disks were exposed to gas with 10% H₂/balance He and 20, 30, or 40 ppm H₂S to determine the H₂S concentration for the Pd/Pd₄S phase boundary at 500, 550, and 600°C. The ANL-3e disks for the tests were made by uniaxially hot-pressing (25 min at 1150°C under a mechanical pump vacuum) a powder mixture of 60 vol. % Pd (Technic) and TZ-3Y powder (Tosoh). To determine whether TZ-3Y affects the chemical stability of Pd in ANL-3e membranes, palladium foil samples were used as a control.

The ANL-3e thin-film membranes were prepared from a mixture of 50-60 vol. % Pd (Technic), TZ-3Y (Sigma Aldrich, submicron particle size), and either manganese oxide or cobalt nitrate as a sintering aid. Blending the powder mixture with an organic binder

and solvent produced an ink that was used to paint a thin film onto a pre-sintered substrate. Substrates were prepared by mixing TZ-3Y powder (Sigma Aldrich submicron powder) with an organic binder and 5-10 mol. % sintering aid (relative to TZ-3Y). Carbon black from Fisher Scientific (20 wt. %) and PMMA-CE (Sigma Aldrich, 8 μm) were added as pore formers, and the powder mixture was uniaxially pressed (5-7 kpsi) into a disk. The pore formers were eliminated by pre-sintering the disk for 6-8 h at 900-950°C in air. After the pre-sintered substrate was painted with ink made from membrane components, it was dried in air and then sintered for 4-6 h at 1160-1230°C in air.

Samples were placed inside an open alumina tray at the center of the test reactor, where a thermocouple monitored the temperature. Samples were slowly (2-3°C/min) heated to the test temperature under flowing high purity helium. When the test temperature was reached, the feed gas was switched to the selected composition. After samples were exposed to a test condition for 20-96 h, the feed gas was switched to high purity helium, which flowed (150 ml/min) for 1 h before the samples were quenched to room temperature by quickly (\approx 5-10 s) pulling them to the end of the reactor tube. Samples were then examined by SEM and EDS to determine if Pd₄S had formed.

The total feed-gas flow rate was kept constant (120-125 ml/min) during the tests. It was quantified once or twice each day using a calibrated flow meter (Agilent Optiflow 630 or 570). The feed gas composition was adjusted by using the MKS 1179A mass flow controllers to blend high purity hydrogen (99.995%), ultra purity helium (99.998%), and 100 or 463 ppm H₂S/balance helium. All gases were supplied by Airgas Inc.

Figure 13 shows Pd foil and ANL-3e membrane samples after they were exposed to feed gas with 20-30 ppm H₂S. The surface roughness of the Pd foil increased as lumpy patches of Pd₄S formed on the originally smooth surface. A thin (\approx 10 μm) dense film formed on the exposed surface of the ANL-3e sample. The EDS results showed that the coating's composition was \approx Pd₄S. Examining the ANL-3e membrane's top surface showed small TZ-3Y particles engulfed by a growing layer of Pd₄S. Short (20-24 h) exposures of Pd foil and ANL-3e samples to 30-40 ppm H₂S gave similar results.

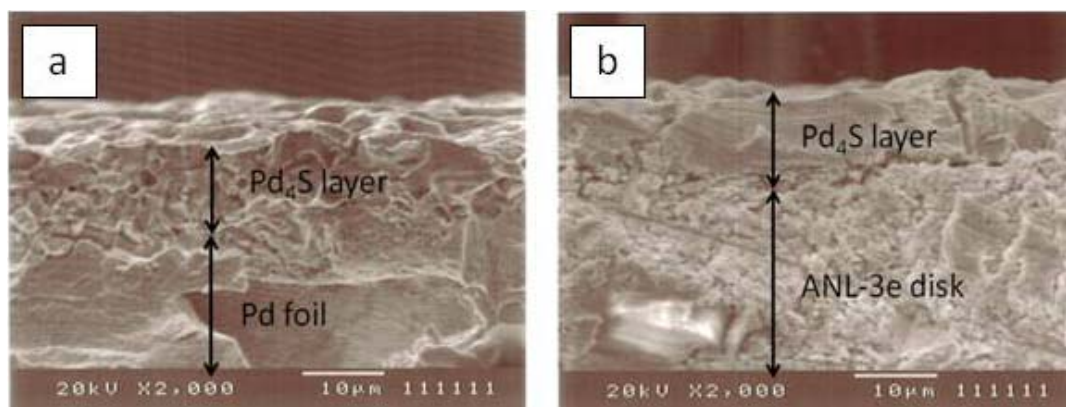


Fig. 13. Secondary electron images of samples after their exposure at 500°C to feed gas with 10% H₂: (a) Pd foil after 72 h in feed with 20 ppm H₂S and (b) ANL-3e disk after 96 h in feed with 30 ppm H₂S.

Figure 14 shows the cross section of an ANL-3e membrane after exposure for 72 h to feed gas with 20 ppm H_2S . The cross section is typical for an ANL-3e membrane that has decomposed to form Pd_4S on its surface. Three distinct bands are evident: a light-shaded layer of Pd_4S at the bottom (near the exposed surface), a $\approx 10\text{-}\mu\text{m}$ -thick darker layer closer to the middle, and a layer with both light and dark areas at the top. The EDS results confirmed that the light-shaded areas are Pd and the dark-shaded areas are TZ-3Y. Thus, the darker layer near the middle was largely depleted of Pd, which had diffused to the surface during the formation of Pd_4S . In contrast, the Pd content of the top layer was similar to that for an unexposed ANL-3e membrane. Based on SEM images such as those in Figs. 13 and 14, the Pd/ Pd_4S phase boundary was approximated experimentally at specific temperatures and $\text{H}_2/\text{H}_2\text{S}$ concentrations using Pd foil, ANL-3e samples, and ANL-3e thin films made with sintering aids.

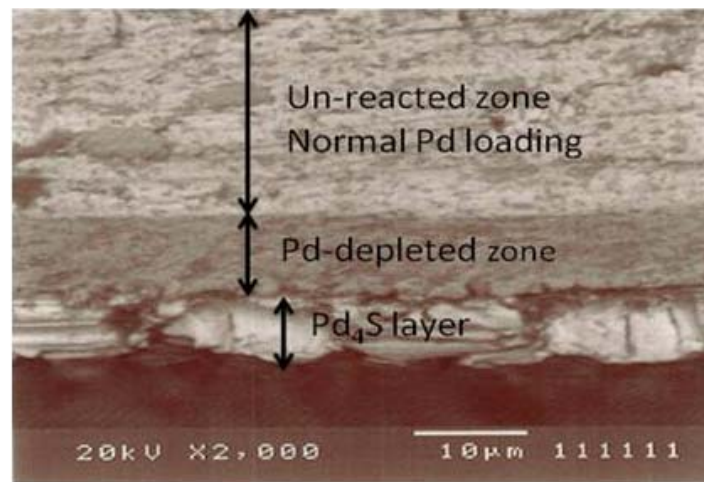


Fig. 14. Backscattered electron image from cross section of ANL-3e disk after its exposure to feed with 10% H_2 and 20 ppm H_2S for 72 h at 500°C showing zone depleted by Pd that diffused to surface (at bottom) to form Pd_4S layer. Bright area is Pd, grey area is TZ-3Y.

Figure 15 shows the FY 2009 results determined previously by experiment and by calculation using thermodynamic parameters derived from the experimental data [2]. The lines are calculated and give the temperatures at which Pd and Pd_4S are in equilibrium for given H_2 and H_2S concentrations; at higher temperature, Pd is stable and Pd_4S unstable, whereas Pd_4S is stable and Pd unstable at lower temperature. Lines were calculated for gas with 73% H_2 and with 10% H_2 to illustrate the effect of hydrogen concentration (through the $\text{H}_2/\text{S}_2/\text{H}_2\text{S}$ equilibrium) on the phase boundary. Points with horizontal bars were determined by examining Pd foil and ANL-3e samples after they were equilibrated in $\text{H}_2/\text{H}_2\text{S}$ mixtures at specific temperatures. The low-temperature end of the bar gives the highest temperature at which Pd_4S was found, and the high-temperature end shows the lowest temperature at which Pd_4S was not found; the Pd/ Pd_4S phase boundary lies between these two temperatures. For example, the phase boundary for samples exposed to 10% $\text{H}_2/8$ ppm $\text{H}_2\text{S}/\text{balance He}$ lies in the range 450-475°C. The results obtained during

FY 2009 are shown by points for thin-film samples and points with vertical bars at 500, 550, and 600°C for hot-pressed disks and Pd foil samples. The vertical bars define ranges of H₂S concentrations, within which the stable phase is unknown without performing additional experiments but above which Pd₄S is stable and below which Pd is stable. Points for thin-film samples show the lowest H₂S concentration at which Pd₄S was found.

As seen in Fig. 15, Pd₄S formed on the surface of Pd foil and ANL-3e samples during their exposure to 10 ppm H₂S at 500°C, but Pd₄S was not found after their exposure to 5 ppm H₂S for 150 h. Figure 16 shows an ANL-3e sample that was exposed to 10 ppm H₂S for 96 h at 500°C, and (as a reference) one that was not exposed to H₂S-containing feed gas. The lighter-shaded phase is Pd in Fig. 16a and Pd₄S in Fig. 16b, whereas the darker-shaded phase in both figures is TZ-3Y. Nearly the entire surface of the ANL-3e sample was covered with Pd₄S after exposure to 10 ppm H₂S at 500°C, leaving only isolated “islands” where TZ-3Y grains were visible. At 550°C, the phase boundary shifted to higher H₂S concentration, with Pd₄S forming under 20 ppm H₂S but not under 10 ppm H₂S. At 600°C, Pd₄S formed when the feed gas contained 20 ppm H₂S but not when the feed gas had 15 ppm H₂S.

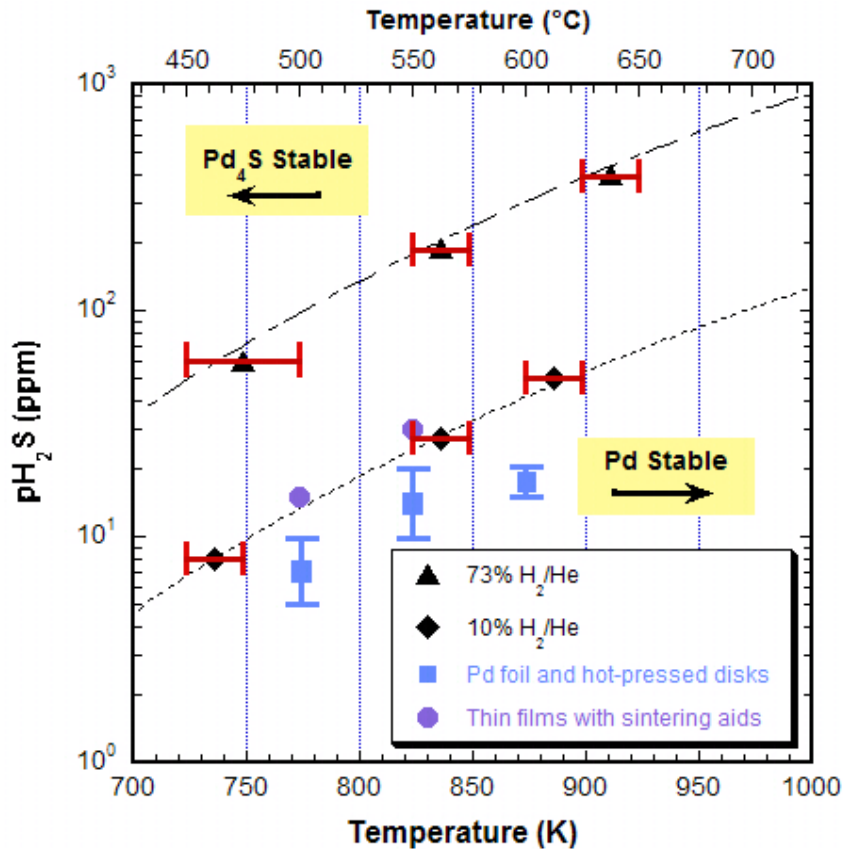


Fig. 15. Partial pressure of H₂S versus temperature showing Pd/Pd₄S phase boundary determined using Pd foil, ANL-3e disks, and ANL-3e thin films made with sintering aids. Curves calculated using thermodynamic parameters derived from the experimental data [2].

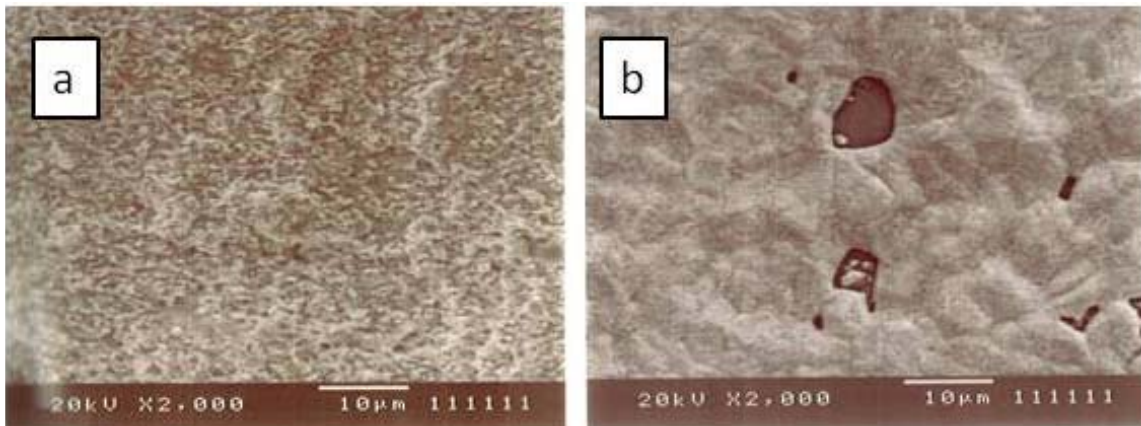


Fig. 16. Plan views of hot-pressed ANL-3e disks: a) after preparation, without any exposure to H₂S-containing atmosphere and b) after 96 h at 500°C under 10 ppm H₂S in 10% H₂/balance He.

The results obtained during FY 2009 with Pd foil and ANL-3e samples (Fig. 15) seem to differ slightly from our previous results [2]. The FY 2009 results indicate that Pd₄S forms at 10 ppm H₂S and 500°C, but the phase boundary calculated previously indicates that Pd remains stable to slightly higher H₂S concentration (≈ 15 ppm). Likewise, the FY 2009 results show that Pd₄S forms at 20 ppm H₂S and 550°C, but the calculated phase boundary suggests that Pd is stable up to ≈ 25 ppm H₂S. Although the differences are small at the lower temperatures, they are larger at 600°C. The FY 2009 results indicate that Pd₄S forms at 20 ppm H₂S, but the calculated boundary suggests that Pd is stable at concentrations up to ≈ 40 ppm H₂S. These apparent differences might be related to kinetic factors, however, because results were obtained during FY 2009 from exposures that lasted from 96-166 h, whereas the previous results were obtained from exposures that lasted only 48 h. Formation of Pd₄S might not have been evident in shorter tests if the formation kinetics were sluggish.

Tests with thin-film samples (Table 8) also suggest that kinetics might have influenced the Pd₄S/Pd phase boundary results. After exposure to 20 ppm H₂S at 500°C for 96 h, Pd₄S was not detected on the surface of thin-film samples made with sintering aid. The absence of Pd₄S suggested that the Pd-Pd₄S phase boundary might be at a slightly higher H₂S concentration for thin films made with sintering aid. After a thin film made with sintering aid was held in feed with 15 ppm H₂S at 500°C for 192 h, however, Pd₄S was detected. The latter result agrees with our previous results [2, 9] and illustrates the importance of kinetics in determining the phase boundary. Also in agreement with our previous results, Pd₄S formed on the surface of thin-film samples with sintering aid after exposure to feed with 30 ppm H₂S at 550°C.

Table 8. Summary of Pd/Pd₄S phase boundary study with ANL-3e thin films.

Test Conditions	Samples Tested	Observations
20 ppm H ₂ S/500°C/96 h	Thin film with Mn oxide Thin film with Co nitrate	Pd ₄ S not evident
15 ppm H ₂ S/500°C/192 h	Thin film with Mn oxide Thin film with Co nitrate Hot-pressed without sintering aid	Pd ₄ S isolated on thin films, nearly continuous on hot-pressed sample
30 ppm H ₂ S/550°C/96 h	Thin film with Mn oxide Thin film with Co nitrate Thin film without sintering aid	Larger Pd ₄ S particles on film made without sintering aid

The kinetics of Pd₄S formation for various types of ANL-3e samples (sintered and hot-pressed disks made without sintering aids and thin films made with and without sintering aids) appears to depend on the preparation conditions for the samples. Figure 17 compares reaction products for ANL-3e thin films made with a sintering aid (Fig. 17a) and without a sintering aid (Fig. 17b) after their exposure to 30 ppm H₂S for 96 h at 550°C. The Pd₄S formation seems more advanced on the film made without a sintering aid, as the Pd₄S particles are noticeably larger. The growth of Pd₄S requires diffusion of Pd from the membrane's interior, indicating faster Pd diffusion in the sample made without sintering aid. Faster Pd diffusion in a film made without a sintering aid seems reasonable, because such a film should have more porosity, which should assist Pd diffusion. Differences are also evident in the Pd₄S reaction products on a hot-pressed ANL-3e disk made without a sintering aid (Fig. 18a), a thin film made with manganese oxide (Fig. 18b), and a thin film made with cobalt nitrate (Fig. 18c) after their exposure to feed with 15 ppm H₂S for 192 h at 500°C. Whereas a continuous layer of Pd₄S covered the hot-pressed sample, only isolated Pd₄S particles were seen on the thin-film samples.

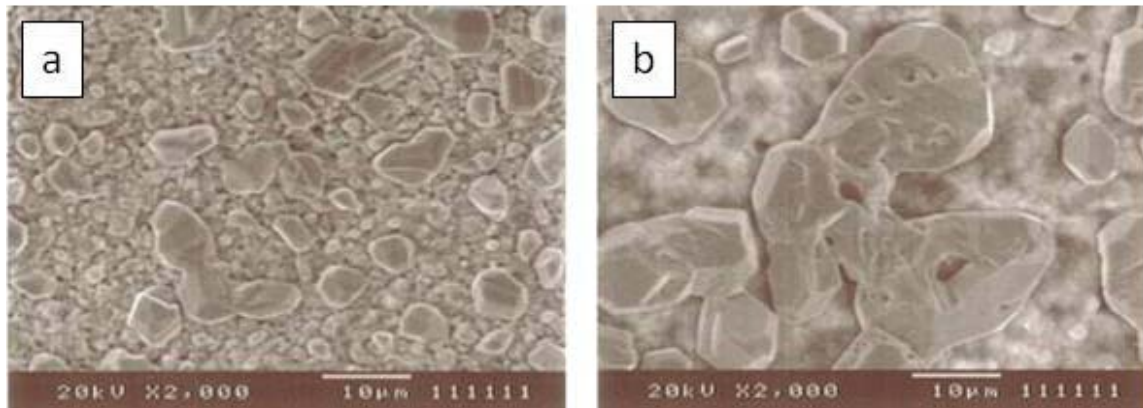


Fig. 17. Secondary electron images showing Pd₄S growth on ANL-3e thin films after 96 h in 10% H₂/30 ppm H₂S at 500°C: a) thin film made with cobalt nitrate sintering aid on TZ-3Y substrate and b) thin film made without sintering aid on porous Al₂O₃ substrate.

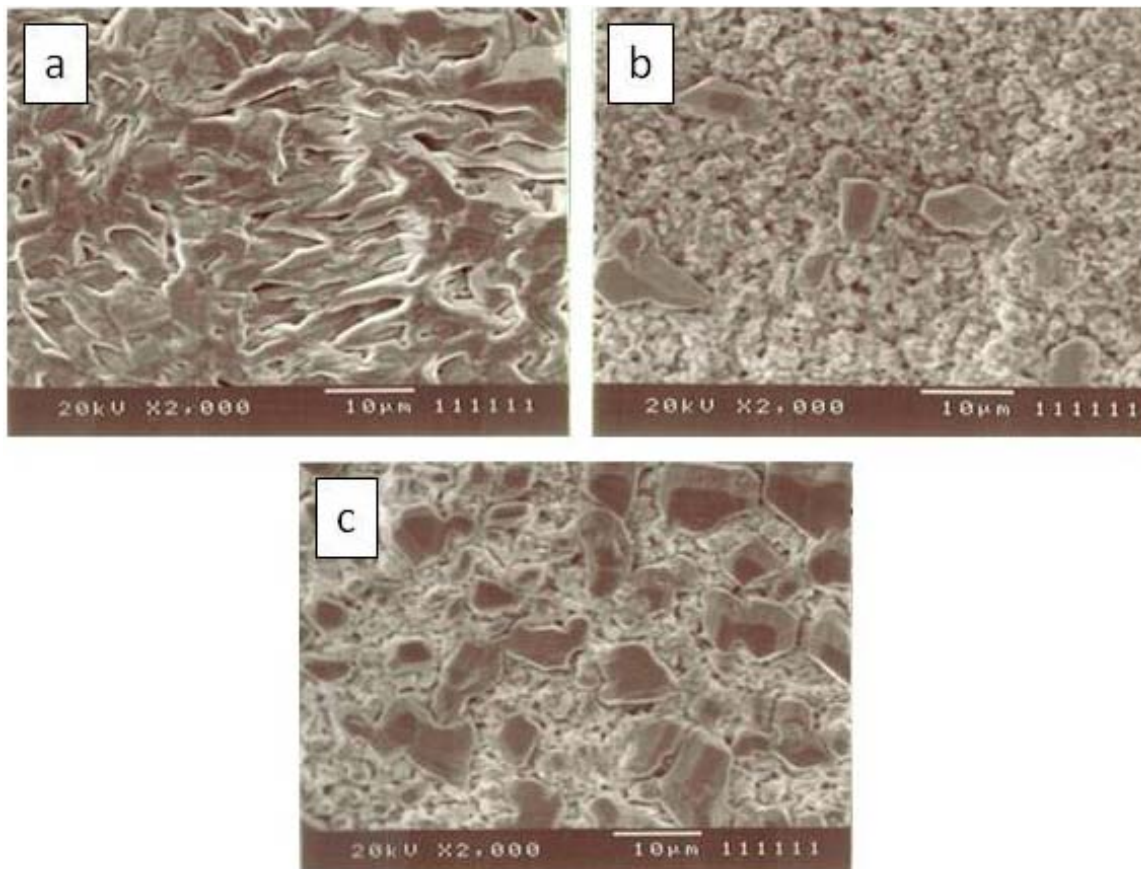


Fig. 18. Secondary electron images showing Pd₄S growth on various types of ANL-3e samples: a) hot-pressed disk without sintering aid, b) ANL-3e thin film with manganese oxide sintering aid and c) ANL-3e thin film made with cobalt nitrate sintering aid.

Various types of ANL-3e membranes and Pd foil give similar results regarding the position of the Pd/Pd₄S phase boundary, but they exhibit differences in behavior during the formation of Pd₄S. The Pd₄S formation reaction seems considerably more sluggish on thin films made with sintering aids than on samples made without sintering aids, probably due to differences in density. Because the extent to which Pd₄S covers a membrane's surface determines how quickly and how badly its flux is degraded, different types of ANL-3e membranes might exhibit significantly different responses to the formation of Pd₄S. Previous measurements at 725°C [3] suggested that the flux of ANL-3e membranes decreased at ≈150 ppm H₂S (due to Pd₄S formation), but the flux of Pd foil showed a decrease at only ≈100 ppm H₂S. To determine whether various types of membrane exhibit practical differences in Pd₄S-formation kinetics that might affect their resistance to attack by H₂S, we will monitor the flux of various membranes during the formation of Pd₄S.

V. FUTURE WORK

Development of Tubular HTMs. We will work to improve the properties of tubular HTMs. Although HTM tubes can be fabricated as either self-supporting tubes composed entirely of HTM components or as thin films on porous tubular supports, we will focus on improving HTM thin films on porous supports, because they have produced the most promising results. Paste painting is an effective method for depositing HTM thin films, but the incidence of pinholes increases as the membrane area increases. We will try to eliminate pinholes either by adding a sintering aid to increase the density of the thin film or by using a modified electroless plating technique to seal the pinholes. Tests will compare the hydrogen flux and helium leakage through thin-film membranes made with cobalt nitrate and manganese oxide as the sintering aid. We will continue testing the performance of tubular HTMs in gases that simulate the atmosphere in "real-life" gasifiers. This might include testing HTM tubes in Argonne's high pressure reactor according to the test protocol developed at the 2008 contractor's review meeting at NETL. The hydrogen flux and permeability of tubular membranes will be measured as a function of sweep and feed gas flow rates to determine whether concentration polarization is a factor.

Membrane Stability. To determine whether various types of membrane exhibit practical differences in Pd₄S-formation kinetics that might effectively improve their resistance to attack by H₂S, we will monitor the flux of various membranes during the formation of Pd₄S. We will correlate hydrogen flux measurements with Pd/Pd₄S phase boundary data in order to better understand the effect of H₂S-containing atmospheres on the performance of HTMs. Correlations will be made between flux and phase boundary data collected at low temperatures (<700°C). In particular, we will compare the hydrogen flux when Pd₄S is stable to that when Pd is stable. To compare the behavior of Argonne's cermet membranes to metallic membranes, we will measure the hydrogen flux for both cermet and metallic membranes on both sides of the phase boundary.

High-Pressure Testing. We will continue using Argonne's high-pressure reactor to test Argonne's membranes according to the established HTM test protocol. Because previous high-pressure measurements indicated that the flow rates of feed and sweep gases influence the flux under some conditions, we will investigate the effects of sweep and feed gas flow rates during our high-pressure flux measurements. Tests according to Test Phase 1 will be completed, and tests according to Test Phase 2 will begin. Tests of tubular HTMs will begin after testing of thin disk-type membranes has been completed.

System Analyses. A third party will be identified by DOE and will evaluate the economics of an integrated gasification and combined cycle (IGCC) system for hydrogen production that employs HTMs for hydrogen purification. In the evaluation, the economics of an IGCC system operating at 900°C will be compared to one operating at 400°C. In addition to identifying novel equipment, estimating its cost, and considering challenges with interfacing the equipment with the overall system, opportunities to improve the overall process will be explored. In particular, heat source temperature,

pressure and duty requirements, heat carrier medium, and conditions and purity of the process streams will be considered. While most of the plant will be based on well-understood equipment, user modules for the HTM units will need to be developed, because HTMs represent a departure from commonly used equipment.

Evaluation of process issues and economics will continue as technical progress warrants. As directed through consultations with NETL's program managers, contacts will be made and discussions will be held with potential collaborators. We will work with NETL's in-house R&D team and their Systems Engineering Group to validate the process concept and conduct techno-economic evaluation of proton-conducting membrane technology for separating hydrogen in the power and petrochemical industries. We will provide technical input and engineering data to the NETL team to develop models for process viability and for thermal management studies.

VI. PUBLICATIONS AND PRESENTATIONS

Transport Properties of $\text{BaCe}_{0.95}\text{Y}_{0.05}\text{O}_{3-\alpha}$ Mixed Conductors for Hydrogen Separation, *Solid State Ionics*, 100, 45 (1997).

Development of Mixed-Conducting Oxides for Gas Separation, *Solid State Ionics*, 108, 363 (1998).

Development of Proton-Conducting Membranes, presented at the AIChE Annual Meeting, New Orleans, LA, March 9-13, 1998.

Mixed-Conducting Ceramic Membranes for Hydrogen Separation, presented at the 193rd Meeting of the Electrochemical Society, San Diego, CA, May 3-8, 1998.

Development of Mixed-Conducting Ceramic Membranes for Hydrogen Separation, *Ceramic Transactions*, 92, 1 (1998).

Development of Mixed-Conducting Dense Ceramic Membranes for Hydrogen Separation, Proc. 5th Intl. Conf. Inorganic Membranes, Nagoya, Japan, June 22-26, 1998, pp. 192-195.

Development of Proton-Conducting Membranes for Hydrogen Separation, presented at the Advanced Coal-based Power and Environmental Systems '98 Conference, Morgantown, WV, July 21-23, 1998.

The Effects of Dopants and A:B Site Nonstoichiometry on Properties of Perovskite-Type Proton Conductors, *J. Electrochem. Soc.*, 145, 1780 (1998).

Transport Properties of $\text{SrCe}_{0.95}\text{Y}_{0.05}\text{O}_{3-\alpha}$ and its Application for Hydrogen Separation, *Solid State Ionics*, 110, 303 (1998).

High-Temperature Deformation of $\text{BaCe}_{1-x}\text{Y}_x\text{O}_{3-y}$ ($0.05 < x < 0.2$), *Solid State Ionics*, 117, 323 (1999).

Development of Mixed-Conducting Ceramics for Gas Separation Applications, *Mat. Res. Soc. Symp. Proc.*, 548, 545 (1999).

Performance Testing of Hydrogen Transport Membranes at Elevated Temperatures and Pressures, presented at Symposium on Hydrogen Production, Storage, and Utilization, New Orleans, Aug. 22-26, 1999; Am. Chem. Soc., Fuel Chem. Div., 44(4), 914 (1999).

Development of Mixed-Conducting Ceramic Membrane for Hydrogen Separation, presented at Sixteenth Annual International Pittsburgh Coal Conference, Pittsburgh, PA, Oct. 11-15, 1999.

Characterization of Ceramic Hydrogen Separation Membranes Containing Various Nickel Concentrations, presented at the Conference on Fossil Energy Materials -- Critical Supporting Technology R&D for Vision 21, Knoxville, TN, April 24-25, 2000.

Mixed Proton-Electron Conducting Cermet Membranes for Hydrogen Separation, presented at 102nd Annual Mtg. of the American Ceramic Society, St. Louis, MO, April 30-May 3, 2000.

Effect of Surface Modification on Hydrogen Permeation of Ni-BaCeO₃ Composites, presented at 102nd Annual Mtg. of the American Ceramic Society, St. Louis, MO, April 30-May 3, 2000.

Effect of Surface Modification on Hydrogen Permeation of Ni-BaY_xCe_{1-x}O_{3-δ} Composites, presented at 197th Meeting of the Electrochemical Society, Toronto, Ontario, Canada, May 14-19, 2000.

Evaluation and Modeling of a High-Temperature, High Pressure, Hydrogen Separation Membrane for Enhanced Hydrogen Production from the Water-Gas Shift Reaction, in "Advances in Hydrogen Energy," eds., C. E. G. Padro and F. Lau, Kluwer Academic/Plenum, New York, pp. 93-110 (2000).

Characterization of Ceramic Hydrogen Separation Membranes with Varying Nickel Concentrations, J. of Applied Surface Science, 167, 34 (2000).

The Crystal Structures and Phase Transitions in Y-doped BaCeO₃: Their Dependence on Y-Concentration and Hydrogen Doping, Solid State Ionics, 138, 63 (2000).

Development of Dense Ceramic Membranes for Hydrogen Separation, Proc. 26th International Conference on Coal Utilization and Fuel Systems, Clearwater, FL, March 5-8, 2001, pp. 751-761.

Thin-Film Cermet Membrane Preparation for Hydrogen Separation, presented at 103rd Annual Meeting of the American Ceramic Society, Indianapolis, IN, April 22-25, 2001.

Surface Modifications of Hydrogen-Separation Membranes Based on the Mixed Conductor Ni-BCY, presented at 103rd Annual Meeting of the American Ceramic Society, Indianapolis, IN, April 22-25, 2001.

Development of Dense Ceramic Membranes for Hydrogen Separation, published in the Proceedings of the 6th Natural Gas Conversion Symposium, Girdwood, Alaska, June 17-22, 2001.

Development of Dense Ceramic Membranes for Hydrogen Separation, Proceedings of the 18th International Pittsburgh Coal Conference, Newcastle, Australia, Dec. 4-7, 2001, published by the Pittsburgh Coal Conference, University of Pittsburgh, Pittsburgh, PA.

Defect Chemistry Modeling of High-Temperature Proton-Conducting Cerates, *Solid State Ionics*, 149, 1 (2002).

Current Status of Dense Ceramic Membranes for Hydrogen Separation, Proceedings of the 27th International Technical Conference on Coal Utilization and Fuel Systems, Clearwater, FL, March 4-7, 2002, published by the Coal Technology Association, Gaithersburg, MD.

Dense Ceramic Membranes for Hydrogen Separation, presented at the 16th Annual Conference on Fossil Energy Materials, Baltimore, MD, April 22-24, 2002.

Hydrogen Production by High-Temperature Water Splitting Using Mixed Oxygen Ion-Electron Conducting Membranes, Proc. 201st Electrochem. Soc. Mtg., Philadelphia, PA, May 12-17, 2002.

Effect of Pd Coating on Hydrogen Permeation of Ni-Barium Cerate Mixed Conductor, *Electrochemical and Solid-State Letters*, 5(3), J5 (2002).

Electrical Properties of p-type Electronic Defects in the Protonic Conductor $\text{SrCe}_{0.95}\text{Eu}_{0.05}\text{O}_{3-\delta}$, *J. Electrochem. Soc.*, 150(6), A790 (2003).

Interfacial Resistances of Ni-BCY Mixed-Conducting Membranes for Hydrogen Separation, *Solid State Ionics*, 159, 121 (2003).

Defect Structure and n-Type Electrical Properties of $\text{SrCe}_{0.95}\text{Eu}_{0.05}\text{O}_{3-\delta}$, *J. Electrochem. Soc.*, 150, A1484 (2003).

Hydrogen Production by Water Splitting Using Mixed Conducting Membranes, Proc. National Hydrogen Assoc. 14th Annual U.S. Hydrogen Meeting, Washington, DC, March 4-6, 2003.

Current Status of Mixed-Conducting Ceramic Membranes for Gas Separation Applications, presented at the Univ. of Houston, March 14, 2003.

Dense Cermet Membranes for Hydrogen Separation, presented at the 225th Amer. Chem. Soc. Natl. Mtg., Fuel Chemistry Div., New Orleans, March 23-27, 2003.

Hydrogen Production by Water Dissociation Using Mixed-Conducting Membranes, presented at 225th Amer. Chem. Soc. Natl. Mtg., Fuel Chemistry Div., New Orleans, March 23-27, 2003.

Current Status of Mixed-Conducting Ceramic Membranes for Gas Separation Applications, presented at the University of Illinois, Urbana-Champaign, April 24, 2003.

Hydrogen Production by Water Dissociation Using Oxygen-Permeable Cermet Membranes, presented at 105th Ann. Mtg. of Amer. Ceramic Soc., Nashville, April 27-30, 2003.

Preparation and Characterization of New Mixed Conducting Oxides $\text{Ba}(\text{Zr}_{0.8-x}\text{Pr}_x\text{Y}_{0.2})\text{O}_{2.9}$, presented at 105th Ann. Mtg. of Amer. Ceramic Soc., Nashville, April 27-30, 2003.

Metal/Ceramic Composites with High Hydrogen Permeability, U.S. Patent #6,569,226, May 27, 2003.

Current Status of Dense Cermet Membranes for Hydrogen Separation, presented at the 20th Annual Intl. Pittsburgh Coal Conf., Pittsburgh, Sept. 15-19, 2003; in Conf. Proc., S46, 187.PDF, 2003.

Current Status of Ceramic Membranes for Hydrogen Production and Separation Applications, presented at the U. of Alaska-Fairbanks, Sept. 24, 2003.

Hydrogen Production by Water Dissociation Using Mixed Conducting Membranes, presented at Second Information Exchange Meeting on Nuclear Production of Hydrogen, Argonne Natl. Lab., Oct. 2-3, 2003.

A Method to Remove Ammonia using a Proton-Conducting Membrane, U.S. Patent #6,630,116, Oct. 7, 2003.

Numerical Modeling of Hydrogen Permeation in Chemical Potential Gradients, Solid State Ionics, 164, 107 (2003).

Development of Dense Cermet Membranes for Hydrogen Separation, presented at the 204th Mtg. of the Electrochemical Soc., Orlando, Oct. 12-17, 2003.

Hydrogen Permeation of Cermet Ba(Ce_{0.6}Zr_{0.2})Y_{0.2}O₃/Ni Membranes, presented at the 204th Mtg. of the Electrochemical Soc., Orlando, Oct. 12-17, 2003.

Hydrogen Permeability of SrCe_{1-x}M_xO_{3-d} (x = 0.05, M = Eu, Sm), Solid State Ionics, 167, 99 (2004).

Use of Mixed Conducting Membranes to Produce Hydrogen by Water Dissociation, Intl. J. Hydrogen Energy, 29, 291-296 (2004).

Hydrogen Production by Water Dissociation using Mixed-Conducting Ceramic Membranes, Proc. of National Hydrogen Assoc. 15th Annual U.S. Hydrogen Energy Conf., Los Angeles, CA, April 27-30, 2004.

Mixed-Conducting Dense Ceramic Membranes for Hydrogen Production and Separation from Methane, presented at 15th World Hydrogen Energy Conf., Yokohama, Japan, June 27-July 2, 2004.

Hydrogen Production from Water Using Mixed-Conducting Ceramic Membranes, presented at 15th World Hydrogen Energy Conf., Yokohama, Japan, June 27-July 2, 2004.

Development of Dense Ceramic Membranes for Hydrogen Production and Separation, Proc. of 8th Intl. Conf. on Inorganic Membranes, eds., F. T. Akin and Y. S. Lin, Adams Press, Chicago, IL (2004), pp. 163-166.

Development of Dense Cermet Membranes for Hydrogen Separation, presented at 21st Annual Intl. Pittsburgh Coal Conf., Osaka, Japan, Sept. 13-17, 2004.

Hydrogen Permeation of Cermet [Ni-Ba(Ce_{0.6}Zr_{0.2})Y_{0.2}O_{3-δ}] Membranes, presented at the 206th Mtg. of the Electrochemical Soc., Honolulu, Oct. 3-8, 2004.

Development of Dense Ceramic Membranes for Hydrogen Production and Separation, presented at American Soc. for Materials--Annual Materials Solution Conf., Columbus, OH, Oct. 18-21, 2004.

Electrical and Hydrogen Transport Properties of SrCe_{0.8}Yb_{0.2}O_{3-δ}/Ni Cermet Membranes, presented at Fall Meeting of Materials Research Society, Boston, Nov. 29-Dec. 3, 2004.

Preparation and Hydrogen Pumping Characteristics of BaCe_{0.8}Y_{0.2}O_{3-δ} Thin Film, presented at Fall Meeting of Materials Research Society, Boston, Nov. 29-Dec. 3, 2004.

Hydrogen Permeability and Microstructure Effect of Mixed Protonic-Electronic Conducting Eu-Doped Strontium Cerate, *J. Mater. Sci.*, **40**, 4061-4066 (2005).

Defect Structure and Transport Properties of Ni-SrCeO_{3-δ} Cermet for Hydrogen Separation Membrane, *J. Electrochem. Soc.* **152**(11), J125 (2005).

Dense Cermet Membranes for Hydrogen Separation, presented at American Institute of Chemical Engineers (AIChE) Spring National Meeting, Atlanta, GA, April 10-14, 2005.

Hydrogen Separation Using Dense Cermet Membranes, presented at 30th Intl. Tech. Conf. on Coal Utilization and Fuel Systems, Clearwater, FL, April 17-21, 2005.

Electrical and Hydrogen Transport Properties of SrCe_{0.8}Yb_{0.2}O_{3-δ}/Ni Cermet Membranes, *Mat. Res. Soc. Symp. Proc.*, **835**, K3.2 (2005).

Preparation and Hydrogen Pumping Characteristics of BaCe_{0.8}Y_{0.2}O_{3-δ} Thin Film, *Mat. Res. Soc. Symp. Proc.*, **835**, K1.5 (2005).

Structure, Proton Incorporation and Transport Properties of Ceramic Proton Conductor Ba(Ce_{0.7}Zr_{0.2}Yb_{0.1})O_{3-δ}, *Mat. Res. Soc. Symp. Proc.*, **835**, K1.4 (2005).

Development of Dense Ceramic Membranes for Hydrogen Separation, presented at 2005 DOE Annual Hydrogen Program Review, Washington, DC, May 23-25, 2005.

Membranes: The Good, The Bad, and The Ugly, presented to Hydrogen & Fuel Cell Tech. Prog. Office, DOE, Wash., DC, June 8, 2005.

Thin Film Preparation and Hydrogen Pumping Characteristics of BaCe_{0.8}Y_{0.2}O_{3-δ}, *Solid State Ionics*, **176**, 1479-1484 (2005).

Hydrogen Production by Water Splitting Using Dense Thin-Film Cermet Membranes, presented at Fall Meeting Materials Research Society, Boston, Nov. 28-Dec. 2, 2005.

Hydrogen Permeation and Chemical Stability of Cermet [Ni-Ba(Zr_{0.8-x}Ce_xY_{0.2})O₃] Membranes, *Electrochem. & Solid State Lett.*, **8**(12), J35-J37 (2005).

Electrochemical Hydrogen Pumping Characteristics of BaCe_{0.8}Y_{0.2}O_{3-δ} Thin Film, presented at Electrochem. Soc. 2005 Fall Mtg., Los Angeles, Oct. 16-21, 2005.

Defect Structure and Transport Properties of Ni-SrCeO_{3-δ} Cermet for Hydrogen Separation Membrane, *J. Electrochem. Soc.*, **152** (11), J125, 2005.

Review: Stress-Induced Diffusion and Cation Defect Chemistry Studies of Perovskites, invited paper published in "Defects & Diffusion in Ceramics – An Annual Retrospective VII: Defect & Diffusion Forum," Scitech Publication, London, UK (Oct. 2005), pp. 43-63.

Hydrogen Production by Water Dissociation Using Mixed Oxygen Ion-Electron Conducting Membranes, presented at Electrochem. Soc. 2005 Fall Mtg., Los Angeles, Oct. 16-21, 2005.

Hydrogen Permeation of Ceramic/Metal Composite Thin Films, presented at Electrochem. Soc. 2005 Fall Mtg., Los Angeles, Oct. 16-21, 2005.

Development of Dense Cermet Membranes for Hydrogen Separation, invited presentation at World Hydrogen Technologies Convention, Singapore, Oct. 3-6, 2005.

Mixed-Conducting Dense Ceramic Membranes for Air Separation and Natural Gas Conversion, *J. Solid State Electrochem.*, 10, 617-624 (2006).

Hydrogen Separation by Dense Cermet Membranes, *Fuel*, 85(2), 150-155 (2006).

Hydrogen Production by Water Dissociation Using Mixed-Conducting Dense Ceramic Membranes, invited presentation at Amer. Chem. Soc. 231st Natl. Mtg., Atlanta, March 26-30, 2006.

Development of Dense Membranes for Hydrogen Production and Separation, Invited Talk at the 2nd Energy Center Hydrogen Initiative Symposium, Purdue University, West Lafayette, IN, April 12-13, 2007.

Development of Dense Cermet Membranes for Hydrogen Separation, presented at AIChE Spring Mtg., Orlando, FL, April 23-27, 2006.

Hydrogen Production from Methane Using Dense Oxygen and Hydrogen Transport Membranes, presented at 209th Electrochemical Soc. Mtg., Denver, May 7-12, 2006.

Development of Dense Hydrogen Transport Membranes, presented at the 31st International Technical Conference on Coal Utilization and Fuel Systems, Clearwater, FL, May 21-25, 2006.

Annealing Effect of Cermet Membranes on Hydrogen Permeability, *Chem. Lett.*, 35(12), 1378-1379 (2006).

Mixed-conducting Membranes for Hydrogen Production and Separation, Invited presentation at 2006 MRS Fall Meeting, Boston, MA, Nov. 27 – Dec. 1, 2006.

Dense Cermet Membranes for Hydrogen Separation from Mixed Gas Streams, presented at 23rd Annual Intl. Pittsburgh Coal Conf., Pittsburgh, PA, Sept. 25-28, 2006.

Effect of Zr-Doping on the Chemical Stability and Hydrogen Permeation of the Ni-BaCe_{0.8}Y_{0.2}O_{3-δ} Mixed Protonic-Electronic Conductor, *Chemistry of Materials*, 18(19), 4647 (2006).

Composite Ni-Ba(Zr_{0.1}Ce_{0.7}Y_{0.2})O₃ Membrane for Hydrogen Separation, *J. Power Sources*, 159(2), 1291 (2006).

Stability of Dense Cermet Membranes for Hydrogen Separation, presented at 211th Meeting of Electrochemical Society, Chicago, IL, May 6-10, 2007.

Development of Dense Membranes for Hydrogen Production from Coal, Invited Talk at 234th American Chemical Society National Meeting, Boston, MA, Aug. 19-23, 2007.

Dense Membranes for Hydrogen Separation and Purification, "Materials for the Hydrogen Economy," ed. by R. H. Jones and G. J. Thomas, Pg. 147, CRC Press LLC, Boca Raton, FL (2007).

Chemical Stability of Hydrogen Transport Membranes, presented at the 24th Annual International Pittsburgh Coal Conference, Johannesburg, South Africa, Sept. 10-14, 2007.

Development of Dense Membranes for Hydrogen Production and Purification, presented at the American Ceramic Society's Materials Innovations in an Emerging Hydrogen Economy, Cocoa Beach, FL, Feb. 24-26, 2008.

Status of Hydrogen Separation Membrane Development, presented at National Hydrogen Assoc. Annual Hydrogen Conf., Sacramento, CA, March 30 – April 4, 2008.

Development of Dense Membranes for Hydrogen Separation from Coal Gasification Streams, presented at AIChE/ACS Spring Meeting, New Orleans, LA, Apr. 6-10, 2008.

Development of Membranes for Purifying Hydrogen Produced by Coal Gasification and/or Methane Reforming, presented at the 25th Annual Intl. Pittsburgh Coal Conf., Pittsburgh, PA, Sept. 29-Oct. 2, 2008.

The Effect of Hydrogen Partial Pressure on Uniaxial Creep of 3Y-TZP/50 vol. % Pd Cermet Membranes, *Materials Science and Engineering B*, 150(3), 145-150 (2008).

Space Charge Potential of Proton-Conducting $\text{BaCe}_{0.8}\text{Y}_{0.2}\text{O}_{2.9-\delta}$, *J. Cer. Process. Res.*, 9(4), 376-380 (2008).

Thickness Dependence of Hydrogen Permeability in $\text{Ni-BaCe}_{0.8}\text{Y}_{0.2}\text{O}_{3-\delta}$, *Solid State Ionics*, 179(33-34), 1854-1857 (2008).

Development of Dense Hydrogen Separation Membranes, presented at National Hydrogen Association Annual Hydrogen Conference, Columbia, SC, March 30-April 3, 2009.

REFERENCES

1. U. Balachandran, Hydrogen Separation Membranes--Annual Report for FY 2006, Argonne National Laboratory.
2. U. Balachandran, Hydrogen Separation Membranes--Annual Report for FY 2007, Argonne National Laboratory.
3. U. Balachandran, Hydrogen Separation Membranes--Annual Report for FY 2008, Argonne National Laboratory.
4. U. Balachandran, Hydrogen Separation Membranes--Quarterly Report for April-June 2009, Argonne National Laboratory.
5. U. Balachandran, Hydrogen Separation Membranes—Quarterly Report for Oct.-Dec., 2008, Argonne National Laboratory.
6. J. L. Shi, T. S. Yen, and H. Schubert, *J. Mat. Sci.*, 32(5), 1341 (1997).
7. G. S. Lewis, A. Atkinson, and B. C. H. Steele, *J. Mat. Sci., Lett.*, 20(12) 1155 (2001).
8. S. Ramesh, C. Gill, and S. Lawson, *J. Mat. Sci.*, 34(22) 5457 (1999).
9. U. Balachandran, Hydrogen Separation Membranes—Quarterly Report for Jan-Mar., 2009, Argonne National Laboratory.



Energy Systems Division

Argonne National Laboratory
9700 South Cass Avenue, Bldg. 212
Argonne, IL 60439-4838

www.anl.gov



U.S. DEPARTMENT OF
ENERGY

Argonne National Laboratory is a U.S. Department of Energy
laboratory managed by UChicago Argonne, LLC